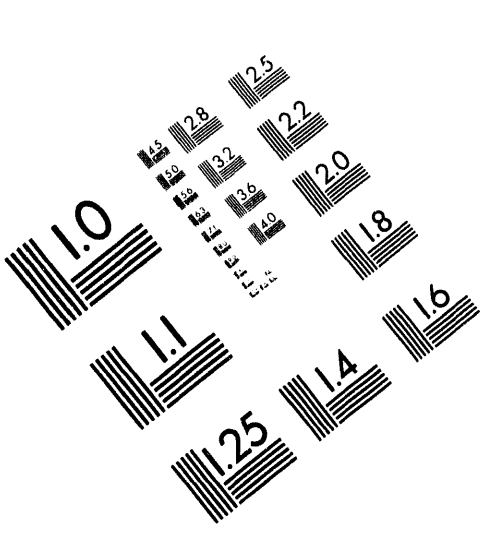

Association for Information and Image Management

1100 Wayne Avenue, Suite 1100
Silver Spring, Maryland 20910

301/587-8202

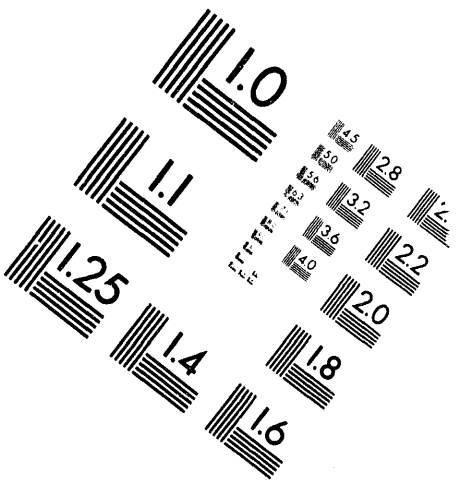

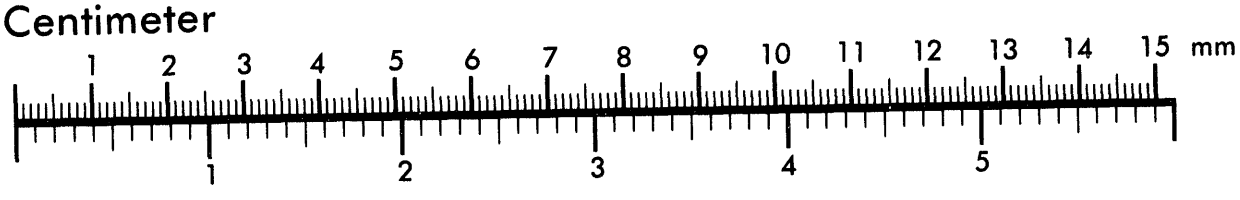

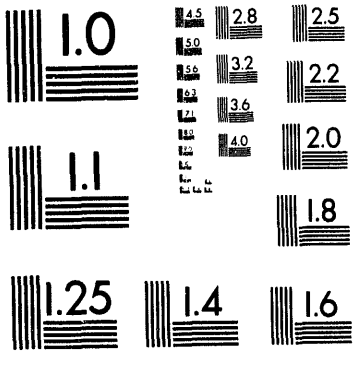

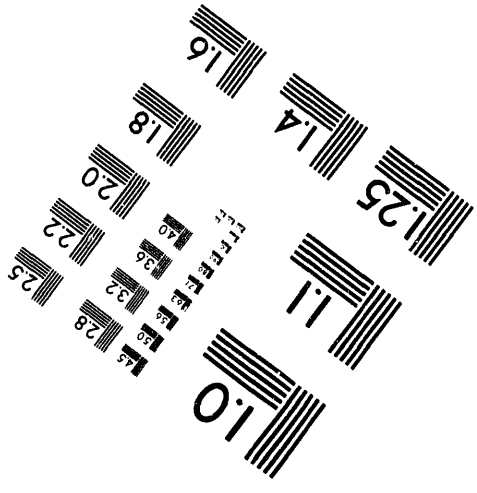

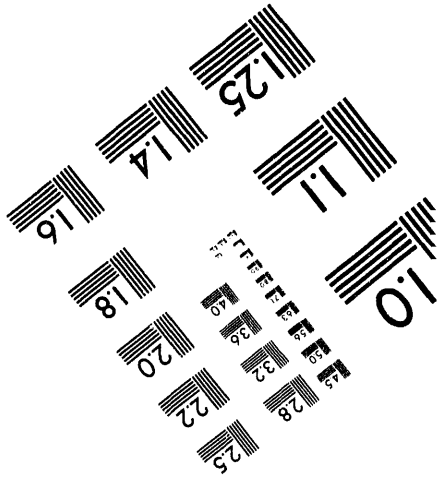

MANUFACTURED TO AIIM STANDARDS
BY APPLIED IMAGE, INC.

1 of 1

Conf-940553--81

UCRL-JC-115351
PREPRINT

The Impact of Buoyant Gas-Phase Flow and Heterogeneity on Thermo-Hydrological Behavior at Yucca Mountain

Thomas A. Buscheck
John J. Nitao

This paper was prepared for submittal to the
American Nuclear Society
International High Level Radioactive Waste Management Conference
Las Vegas, Nevada
May 22–26, 1994

January 1994

Contents

The Impact of Buoyant, Gas-Phase Flow and Heterogeneity on Thermo-Hydrological Behavior at Yucca Mountain

Thomas A. Buscheck and John J. Nitao
Earth Sciences Department, L-206, P.O. Box 808
Lawrence Livermore National Laboratory, Livermore, CA 94551
telephone: (510) 423-9390, (510) 423-0297
fax: (510) 422-3118

Abstract

To safely and permanently store high-level nuclear waste, the potential Yucca Mountain repository system must mitigate the release and transport of radionuclides for tens of thousands of years. In the failure scenario of greatest concern, water would contact a waste package, accelerate its failure rate, and eventually transport radionuclides to the water table. Our analyses have demonstrated that the only significant source of liquid water is fracture flow from: (1) natural infiltration, (2) condensate drainage generated under *boiling conditions*, and (3) condensate drainage generated under *sub-boiling conditions*. The first source of liquid water arises from the ambient system; the second and third sources are generated by repository heat. Buoyant, gas-phase flow, occurring either on a sub-repository scale or on a mountain scale, may play an important role in generating the second and third sources of liquid water. By considering a wide range in bulk permeability of the fractured rock, we identify a threshold bulk permeability at which buoyant, gas-phase convection begins to dominate hydrological behavior. At 10 times this threshold, convection begins to dominate thermal behavior. These effects can dominate moisture movement in the unsaturated zone on the order of 100,000 yr. We find that the development of a large above-boiling zone suppresses the effects of buoyant vapor flow. Zones of sharply contrasting bulk permeability also influence condensate generation and drainage. Of particular concern are conditions that focus vapor flow and condensate drainage, which could result in persistent refluxing at the repository, causing water to drip onto waste packages. These effects can occur under both sub-boiling and boiling conditions. Long-term *in situ* heater tests are required to diagnose the potential for major repository-heat-driven sources of fracture flow.

I. Introduction

The U.S. Department of Energy (DOE) is investigating the suitability of Yucca Mountain as a potential site for the nation's first high-level nuclear waste repository. The site consists of a series of fractured, nonwelded to densely welded tuff units and is located about 120 km northwest of Las Vegas, Nevada, in an area of uninhabited desert.[1] The potential repository location is in Topopah Spring moderately to densely welded tuff, approximately 350 m below the ground surface and 225 m above the water table.[2] Favorable aspects of Yucca Mountain relate primarily to its arid nature, which results in unsaturated conditions at the potential repository horizon.

To safely and permanently store waste, the potential repository system must limit gas- or liquid-phase transport of radionuclides to the accessible environment for tens of thousands of years. In the failure scenario of greatest concern, water would contact a waste package, accelerate its failure rate, and eventually transport radionuclides to the water table. The degradational mechanisms of greatest concern for waste package integrity, such as stress and pitting corrosion or microbial attack, require the presence of liquid water. The rates for many of these degradational mechanisms are enhanced under warm, moist conditions. It should be noted that most of the potential high-level nuclear waste repository sites under consideration by other nations are below the water table in the saturated zone, where 100% of the rock pore space is filled with liquid water. Therefore, for a repository located in the saturated zone, the presence of liquid water is a given, and the degradational mechanisms depend primarily on the geochemistry near the waste packages.

For a repository located in the unsaturated zone, the primary concern is whether liquid water may contact the

waste package. This contact can arise from two effects. First, mobile liquid water, particularly flowing in fractures, may contact the waste package. Second, if the relative humidity of the gas phase is sufficiently high, a liquid film can exist on the surface of the waste package even if mobile liquid water is absent. Note that the relative humidity depends on the temperature and the liquid saturation in the surrounding rock. The liquid saturation is defined as the fraction of the rock pore space that is filled with liquid water. If either the liquid saturation is sufficiently low, or the temperature is sufficiently high, the resulting low relative humidity will substantially reduce the rates of many of the degradational mechanisms. Moreover, even for breached waste packages, waste-form dissolution would be minimal if liquid water is absent.

I.A Major Potential Sources of Fracture Flow

The fractured rock mass at Yucca Mountain consists of fractures and rock matrix. Fluid flow in the unsaturated zone involves the movement of liquid water (the liquid phase) and gas (the gas phase) through the fractures and rock matrix. Under ambient conditions, the gas phase contains about 98.5% air and 1.5% water vapor. Most of the liquid water is tightly held in the pores of the rock matrix by capillary forces. Typically, more than half of the matrix pore space is occupied with liquid water, with the remaining pore space occupied by gas. Except for regions with a perched water table, capillary forces cause most of the fractures to be drained of liquid water; consequently, the fractures are mostly gas filled. In studies of high-level radioactive waste isolation, modeling and theoretical advances in nonisothermal, multiphase flow have demonstrated the critical importance of disequilibrium flow processes between the fractures and the matrix.[3,4] Matrix permeability at Yucca Mountain is extremely small, so matrix flow is of little concern for repository performance. Rather, fracture flow is the most likely means of generating a significant source of mobile liquid water. This water may arise from three potential origins:

(1) natural infiltration of rainfall and snowmelt,

(2) condensate generated under *boiling conditions*, and

(3) condensate generated under *sub-boiling conditions*.

The first source of liquid water arises from the ambient system; the second and third sources are generated by radioactive decay heat, primarily from spent nuclear fuel. Heat-driven, buoyant vapor flow, occurring either on a sub-repository scale or on a mountain scale (Figs. 1a and b), may play an important role in generating the second and third sources of liquid water. Zones of sharply contrasting bulk permeability of the fractured rock mass can also influence vapor and condensate flow, under both boiling and sub-boiling conditions. Of particular concern are conditions that promote the focusing of vapor and condensate flow, which could cause water to drip onto waste packages (Fig. 1c).

Repository heat also drives buoyant, liquid-phase convection in the saturated zone (Fig. 1b). Analyses of this type of flow indicate that it is likely to be the dominant means of driving radionuclide transport in the saturated zone for tens of thousands of years.[6,7] A bulk permeability distribution that facilitates deep convective mixing of radionuclides in the saturated zone would be more likely to meet a dose-based standard than a stagnant water table.

Table I summarizes the time and length scales involved in how repository heat influences the three major sources of fracture flow. Mountain-scale effects depend on the overall heating conditions for the entire repository. We have shown[5–8] that the most useful macroscopic thermal loading parameter quantifying the time-integrated heat content of the waste in the repository is the Areal Mass Loading [(AML), expressed in metric tons of uranium per acre, MTU/acre]. Mountain-scale effects depend primarily on the AML of the entire repository, and they are insensitive to the details of waste package emplacement, such as waste package size and spacing, and fuel age. These effects also depend on the distribution of thermal and hydrological properties throughout the unsaturated zone.

Sub-repository-scale effects depend on the local heating conditions around waste packages. Important factors include (1) the number of spent nuclear fuel assemblies per waste package, (2) the spacing between waste packages, and (3) the age of the spent nuclear fuel. In general, the number of fuel assemblies per waste package is directly related to the waste package size. Larger waste packages are capable of containing a larger number of assemblies; consequently, they have a higher thermal output. Younger fuel has a higher thermal output than older fuel for some period of time. The Local Areal Mass Loading (LAML) depends on the waste package size and spacing. For a given LAML, sub-repository-scale effects are very different, depending on whether widely spaced, large waste packages or tightly spaced, small waste packages are used. These effects also depend on the near-field distribution of thermal and hydrological properties within a few tens of meters of the waste packages.

In addition to generating condensate flow, repository heat can redistribute the liquid saturation in the unsaturated zone, causing regions of dry-out below the repository and liquid saturation buildup above. These changes can impact ambient fracture flow, possibly amplifying the effects of natural infiltration in regions of increased liquid saturation and attenuating those effects in regions of dry-out. These changes, along with temperature changes, can alter the intrinsic hydrological, geochemical, and geomechanical properties that influence fluid flow and radionuclide transport in the unsaturated zone. Our analyses[5–8] have

indicated that repository-heat-driven changes in the saturation distribution can persist for more than 100,000 yr, even for low AMLs that never drive temperatures close to the boiling point.

It is important to note that some of our past repository-scale analyses assume the repository thermal load to be uniformly distributed over a disk-shaped area with areally uniform thermo-hydrological properties.[5–7] The vertical distribution of thermo-hydrological properties was included, assuming the major hydrostratigraphic units are horizontal. Effectively, the results of those calculations are representative of averaged, mountain-scale, thermo-hydrological behavior. In this paper, we examine how the spatial variability of heating conditions and hydrological properties causes local thermo-hydrological behavior to deviate from averaged behavior. We also examine the influence of sub-repository-scale and mountain-scale, buoyant vapor flow on thermo-hydrological behavior for both sub-boiling and above-boiling thermal loads. Soil scientists have observed that gas-phase diffusion of water vapor is enhanced under nonisothermal conditions as compared with soil under isothermal conditions. Accordingly, we also investigate the impact that the diffusion enhancement effect may have on thermo-hydrological behavior at Yucca Mountain.

I.B Heat-Driven Flow Processes

An important feature of the unsaturated zone at Yucca Mountain is its high fracture density. Moreover, the Topopah Spring tuff, which occurs at the potential repository depth, is one of the most densely fractured hydrostrati-

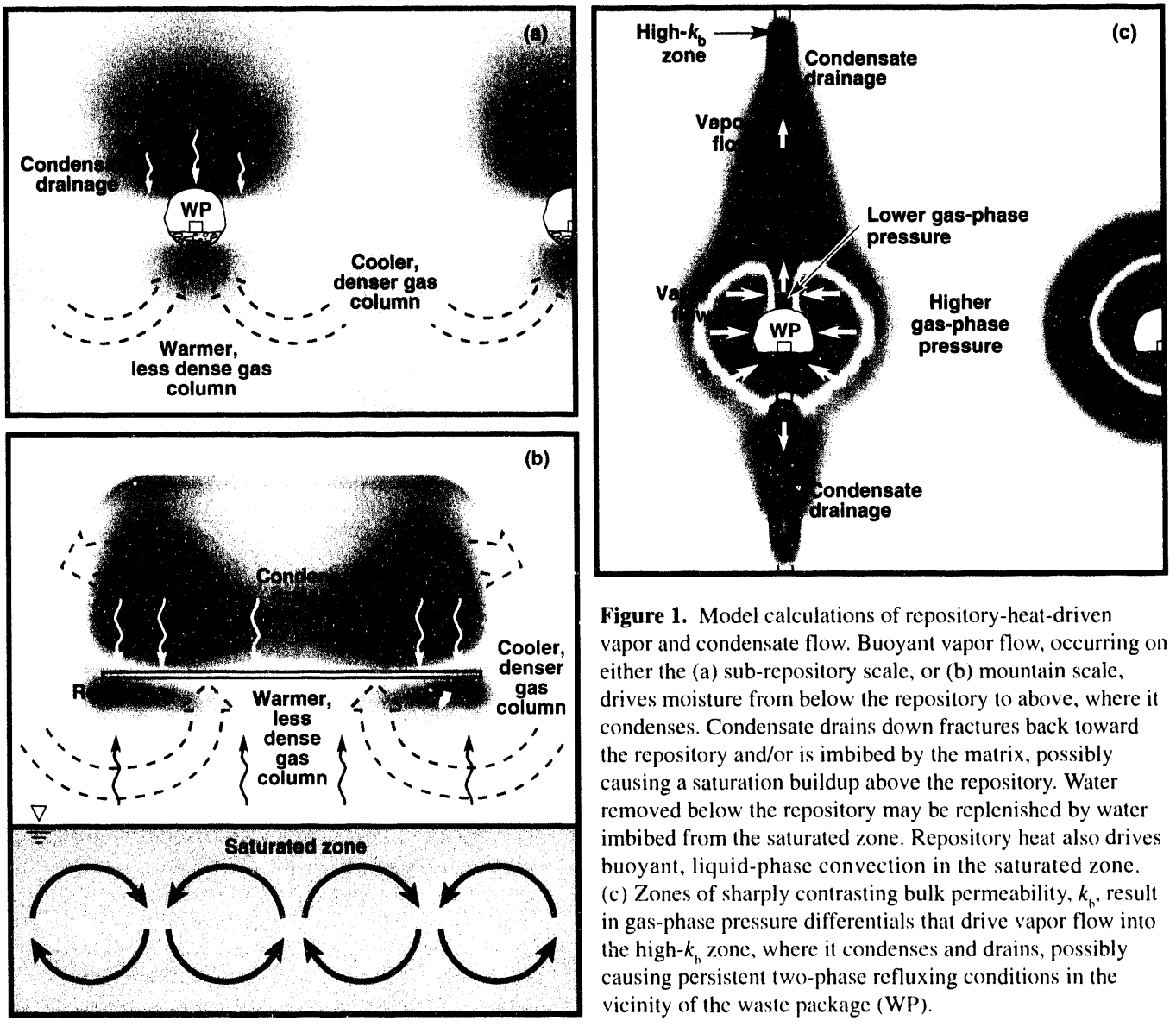

Figure 1. Model calculations of repository-heat-driven vapor and condensate flow. Buoyant vapor flow, occurring on either the (a) sub-repository scale, or (b) mountain scale, drives moisture from below the repository to above, where it condenses. Condensate drains down fractures back toward the repository and/or is imbibed by the matrix, possibly causing a saturation buildup above the repository. Water removed below the repository may be replenished by water imbibed from the saturated zone. Repository heat also drives buoyant, liquid-phase convection in the saturated zone. (c) Zones of sharply contrasting bulk permeability, k_b, result in gas-phase pressure differentials that drive vapor flow into the high-k_b zone, where it condenses and drains, possibly causing persistent two-phase refluxing conditions in the vicinity of the waste package (WP).

graphic units. This is significant because, without fractures, the rock throughout most of the unsaturated zone (including the repository horizon) would be extremely impermeable. In general, repository heat moves moisture by (1) vaporization, (2) driving water vapor from high to low gas-phase pressure, (3) condensation, and (4) gravity- or capillary-driven flow of condensate. Without fractures, the rock would be too impermeable to allow significant vaporization and movement of water vapor. The flow of condensate would also be very slow. A system of connected fractures facilitates significant repository-heat-driven fluid flow as well as natural infiltration. Enhanced gas-phase diffusion of water vapor may significantly contribute to vaporization in unfractured (relatively impermeable) rock.

Heat flow away from the waste packages occurs as heat conduction, the convection of latent and sensible heat, and thermal radiation. Because of the large bulk permeability of fracture networks, gas-phase pressures in the fractures remain very close to atmospheric, even during boiling. Consequently, as temperatures reach the nominal boiling point (≈96°C), boiling first occurs along fractures (Fig. 2) and proceeds into the matrix blocks. Accordingly, dry-out due to boiling is more suppressed in sparsely fractured regions (with large matrix blocks) and less suppressed in intensely fractured regions (with small matrix blocks). As boiling continues, water vapor displaces air away from the waste packages and may replace it completely for sufficiently high AMLs. The question of whether (or how long) air is displaced from the repository is important in assessing the impact of oxidation corrosion on waste package integrity.

Most of the water vapor reaching the fracture network is eventually driven away from the emplacement drift by higher gas-phase pressures in the boiling zone to where cooler temperatures cause it to condense along fracture walls (Fig. 2). Buoyant, gas-phase convection can cause more of the vapor flow to be driven upward to where it condenses above the dry-out zone. In general, regardless of where the condensate is generated, there are three things that can happen to it:

(1) It can drain away from the boiling zone.
(2) It can drain back toward the boiling zone.
(3) It can be imbibed by the matrix.

Table I. The various time and length scales involved in how repository heat influences the three major sources of fracture flow.

Natural infiltration	Buoyant, gas-phase convection and condensate drainage *		Boiling and condensate drainage	
Affected by repository-heat-driven changes to the • moisture distribution • intrinsic hydrological, geochemical, and geomechanical properties	**Sub-repository scale**	**Mountain scale**	**Sub-repository scale**	**Mountain scale**
	Local heating conditions Local Areal Mass Loading Waste package size Waste package spacing	Global heating conditions Areal Mass Loading Repository size Repository location	Local heating conditions Local Areal Mass Loading Waste package size Waste package spacing	Global heating conditions Areal Mass Loading Repository size Repository location
	Near-field thermo-hydrological properties	Unsaturated zone-scale thermo-hydrological properties	Near-field thermo-hydrological properties	Unsaturated zone-scale thermo-hydrological properties
	t < 1000 yr ** t < 2000 yr ***	1000 < t < 100,000 yr	t < 50 yr ** t < 400 yr *** for 27 MTU/acre t < 1000 yr ** for 49 MTU/acre t < 50 yr for 155 MTU/acre	t < 1000 yr t < 100,000 yr for residual effects
	Sub-boiling heater tests	Above-boiling heater tests	Marginal-boiling heater tests	Above-boiling heater tests

* Can occur under both sub-boiling and boiling conditions

** Assuming small waste packages

*** Assuming large waste packages

Because the small matrix permeability limits the rate at which the matrix can imbibe the condensate by capillary suction, it can drain for considerable distances down fractures before being completely imbibed. Below the boiling zone, condensate drainage is away from the boiling zone (Fig. 2), enhancing the dry-out rate. Above the boiling zone, condensate tends to drain back toward the boiling zone, where it reboils, thereby retarding the net rate of dry-out.

The return flow of condensate back toward the heat source causes refluxing, which is the counter-current flow of water vapor and condensate. It is important to note that refluxing does not require boiling conditions.[8] Heat-driven, buoyant gas-phase flow can drive refluxing under sub-boiling conditions. Under boiling conditions, refluxing results in a heat transfer mechanism (driven by the convection of latent heat) called the heat-pipe effect. Given adequately high mass flux rates of water vapor and condensate, heat pipes are capable of sustaining a given heat flux with a much flatter temperature gradient than is associated with heat conduction. Consequently, heat pipes are manifested by a flat temperature profile, with temperatures close to the nominal boiling point. Pruess and others[9,10] were the first to model the heat-pipe effect in the context of thermo-hydrological performance at Yucca Mountain. Depending on the AML, these effects can occur at the sub-repository scale or on a mountain scale (Table I).

Figure 2. Schematic of hydrothermal flow near the emplacement drift. Rock dry-out occurs as boiling drives water vapor out of the rock matrix. Upon reaching the fracture network, vapor is driven away from the boiling zone to where cooler temperatures cause it to condense along fracture walls. Because the small matrix permeability limits the rate of matrix imbibition, condensate drainage persists for considerable distances down fractures.

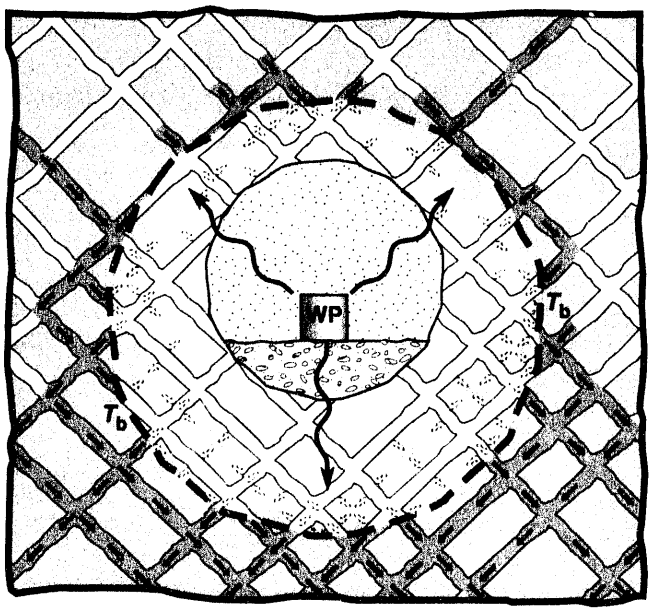

I.C Thermal Loading Strategies

The extent to which the three major sources of fracture flow may impact waste package integrity, waste-form dissolution, and radionuclide migration is critically dependent on site conditions as well as on the thermal loading strategy that will eventually be adopted for the Mined Geological Disposal System (MGDS) at Yucca Mountain. With respect to repository-heat-driven, thermo-hydrological performance, there are three primary thermal loading strategies (or options). These three strategies are best framed as three fundamental questions:

(1) Can the thermal load be limited and distributed such that it has a negligible impact on hydrological performance?

(2) For intermediate thermal loads, will the impact of thermo-hydrological processes and our understanding of those processes allow us to demonstrate that the MGDS meets regulatory compliance?

(3) For higher thermal loads with the potential of generating extended-dry conditions, will the impact of thermo-hydrological processes and our understanding of those processes allow us to demonstrate that the MGDS meets regulatory compliance?

The goal of the first thermal loading strategy is to minimize the hydrological impact of repository heat so that the primary concern in assessing hydrological performance is the ambient hydrological system. Therefore, this strategy requires that (1) we demonstrate that repository heat has a negligible impact on hydrological performance, and (2) the behavior of the ambient hydrological system and our understanding of that behavior are sufficient to demonstrate that the MGDS meets regulatory compliance. The motivation for this strategy is to avoid any potentially adverse effects of repository heat.

The goal of the third thermal loading strategy is to demonstrate that, for some period of time, repository heat is capable of dominating the ambient system with above-boiling conditions surrounding the repository. Ideally, this would result in (1) the absence of liquid water in the vicinity of the waste packages as long as boiling persists, and (2) the continuation of sub-ambient liquid saturation conditions for some time following the above-boiling period without incurring adverse effects that may offset the benefits of dry-out. The primary motivations for this strategy are to (a) minimize the sensitivity of repository performance to hydrological variability, (b) extend the period of radionuclide containment in the engineered barrier system, and, (c) during the period of radionuclide migration, reduce two factors: the probability of water contacting waste packages, and the flow rates associated with transport.

Another important motivation is to delay the period of significant radionuclide migration until the inventory of radionuclides has been substantially diminished by radioactive decay.

The second thermal loading strategy falls between the first and third strategies. All three strategies require an adequate understanding of both the ambient hydrological system and how heat perturbs fluid flow in that system.

It is important to note that what effectively constitutes a "cold," ambient-system-dominated repository or a "hot," extended-dry repository is not well understood. Presently, we lack adequate knowledge of ambient site conditions to define where the transitions from cold to intermediate or from intermediate to hot thermal loads occur. We have analyzed how site conditions will influence the determination of these transitions.[8] In particular, the influence of buoyant, gas-phase convection and how hydrogeological heterogeneity may focus vapor and condensate flow are critical to determining what thermal loads are sufficiently "cold" to render hydrothermal impacts of repository heat as negligible. The influence of these processes will also largely determine what thermal loads are sufficiently "hot" (or whether any such thermal loads exist) to allow us to demonstrate that extended-dry conditions will prevail for some time in the vicinity of waste packages.

Generally speaking, site conditions that are beneficial to a "cold" repository also benefit the performance of a "hot" repository. If we find that the bulk permeability is too small to promote significant buoyant, gas-phase flow and that heterogeneity does not result in significant focusing of vapor flow and condensate drainage, it may be possible to demonstrate that a sub-boiling repository has a negligible impact on the ambient hydrological system. These same site conditions are also beneficial for extending the period of above-boiling temperatures and, during that time, minimizing the presence of mobile liquid water in the vicinity of waste packages.

II. Numerical Models and Assumptions

II.A V-TOUGH Hydrothermal Flow Code

All hydrothermal calculations were carried out using the V-TOUGH (vectorized transport of unsaturated groundwater and heat) code.[11] V-TOUGH is Lawrence Livermore National Laboratory's enhanced version of the TOUGH code, which is a member of the Mulkom family of multiphase, multicomponent codes developed at Lawrence Berkeley Laboratory by Pruess.[12] V-TOUGH is a multidimensional numerical simulator capable of modeling the coupled transport of water, vapor, air, and heat in fractured porous media.

II.B Equivalent Continuum Model (ECM)

Because of the impracticality of discretely accounting for all of the fractures at Yucca Mountain, it was necessary to account for fractures using the ECM. The assumption of capillary pressure and thermal equilibrium between fractures and matrix allows the fracture and matrix properties to be pore-volume-averaged into an equivalent medium. The bulk porosity, ϕ_b, bulk saturation, S_b, and bulk hydraulic conductivity, K_b, of the equivalent medium are given by:

$$\phi_b = \phi_f + (1 - \phi_f)\phi_m \tag{1}$$

$$S_b = \frac{S_f\phi_f + S_m(1 - \phi_f)\phi_m}{\phi_f + (1 - \phi_f)\phi_m} \tag{2}$$

$$K_b = K_m(1 - \phi_f) + K_f\phi_f \tag{3}$$

where ϕ_m, S_m, ϕ_f, and S_f are the porosity and saturation of the matrix and fractures, respectively, and K_m and K_f are the hydraulic conductivities of the matrix and fractures. Because of the small K_m in the unsaturated zone (UZ), K_b is almost completely dominated by K_f and ϕ_f for most fracture spacings and permeabilities.

II.C Thermo-Hydrological Properties

All major hydrostratigraphic units in the UZ at Yucca Mountain are included in the models (Table II).[12,13] The hydrostratigraphic profile employed here has been used in previous modeling studies.[3,5-8] The wet and dry thermal conductivity, K_{th}, data were obtained from the Reference Information Base (RIB).[14] We assume the steady-state liquid saturation profile obtained for a net recharge flux of 0 mm/yr, yielding a repository horizon saturation of 68%.[3]

Table II.
Hydrostratigraphic units in models.

Units	Depth interval (m)
TCw	0 to 30
PTn	30 to 67.4
TSw1	67.4 to 197.5
TSw2	197.5 to 387.5
TSw3	387.5 to 403.4
CHnv	403.4 to 407.9
CHnz	407.9 to 539.6
PPw	539.6 to 568.1

w = welded n = nonwelded v = vitric z = zeolitized

Previous work[5-7] also considered the steady-state saturation profile obtained for recharge fluxes of 0.045 and 0.132 mm/yr, resulting in repository saturations of 85 and 95%, respectively.

The reference case assumed a bulk permeability, k_b, of 2.8×10^{-13} m^2 (280 millidarcy), which is equivalent to three 100-μm fractures per meter. The sensitivity of buoyant, gas-phase convection, boiling and dry-out performance to k_b was examined by considering the following values of k_b: 1.9 microdarcy (no fractures), 10 microdarcy (three 3-μm fractures per meter), 100 microdarcy (three 7-μm fractures per meter), 1 millidarcy (three 15-μm fractures per meter), 10 millidarcy (three 33-μm fractures per meter), 1 darcy (three 153-μm fractures per meter), 5 darcy (three 262-μm fractures per meter), 10 darcy (three 330-μm fractures per meter), 20 darcy (three 416-μm fractures per meter), 40 darcy (one 781-μm fracture per meter), 84 darcy (one 1000-μm fracture per meter), 168 darcy (one 1260-μm fracture per meter), 414 darcy (one 1700-μm fracture per meter), and 840 darcy (one 2150-μm fracture per meter).

II.D Initial and Boundary Conditions

The vertical temperature distribution, T, in the models is initialized to correspond to the nominal geothermal gradient in the region. The atmosphere at the ground surface is represented by a constant-property boundary, with T and gas-phase pressure fixed at 13°C and 0.86 atm, respectively. The relative humidity at the ground surface is also fixed at a value that represents thermodynamic equilibrium with respect to the initial saturation conditions at the top of the TCw unit (see Table II). Therefore, under initial (ambient) saturation and temperature conditions, there is no mass flux of water vapor between the atmosphere and upper TCw. In previous work,[5] it was assumed that because of the large fracture permeability, buoyant convective mixing in the saturated zone (SZ) results in it acting as a heat sink. The large k_b and storativity of the SZ were also assumed to result in the water table being at a fixed depth. For the drift-scale calculations reported here, we also assume that the water table has a fixed depth (z = 568.1 m) and a constant temperature (31°C). The constant-temperature water table assumption causes the water table to act as a heat sink. Because this model does not explicitly model hydrothermal flow in the SZ, it is called the "UZ" model. In comparing the UZ model with the UZ-SZ model, which is described below, we found that, for the first 1000 yr, repository temperatures are insensitive to the treatment of heat flow at the water table.[6,7] Because the primary use of the drift-scale model is to examine sub-repository-scale, thermo-hydrological behavior during the first 1000 yr, the constant-temperature water table assumption does not significantly affect the interpretation of our results. The initial temperature and saturation at the repository horizon in the UZ model are 23.3°C and 68%, respectively.

We conduct most of our calculations with a UZ-SZ model (which includes hydrothermal flow in the upper 1000 m of the SZ). Conductive and convective heat flow, including buoyancy flow, are modeled in the SZ. Because the RIB[14] lacks thermal property and hydrological data below the PPw unit (the lowermost hydrostratigraphic unit in our UZ model), we assumed that the PPw data were applicable to the upper 1000 m of the SZ (down to the lower boundary of the UZ-SZ model). The lower boundary of the UZ-SZ model has a constant temperature of 53.5°C and a fixed pressure corresponding to the hydrostatic pressure and temperature profile of the upper 1000 m of the SZ. The initial temperature and saturation at the repository horizon in the UZ-SZ model are 23.5°C and 68%, respectively.

II.E Repository-Scale Model

For the reference thermal load in the Site Characterization Plan–Conceptual Design Report[15] (SCP-CDR), with 10-yr-old spent nuclear fuel (SNF), an Areal Power Density (APD) of 57 kW/acre, and an AML of 49.2 MTU/acre, we assumed that the heated area of the repository is 1747 acres. For a 1747-acre repository, the repository-scale model represents the repository as a 3-km-diameter, 4.6-m-thick, disk-shaped heat source with a uniformly distributed thermal load. Repository areas of 559, 1118, and 3162 acres were also modeled for AMLs of 154.7, 77.3, and 27.1 MTU/acre, respectively. The model, which is similar to models used by Pruess and Tsang,[16] utilizes an axisymmetric coordinate system centered at the repository center. This model is useful for calculating temperature and saturation behavior (averaged from one emplacement drift to the next) as a function of location relative to the center (or edge) of the repository area. The assumption was also made that the thermal loading of the repository can be represented by the heat generation curve of pressurized water reactor (PWR) SNF of an average age. Calculations were made for APDs ranging from 10 to 114 kW/acre and SNF ages of 10, 20, and 30 yr with a burnup of 33,000 MWd/MTU.

II.F Sub-Repository-Scale Models

Because it areally averages the thermal load, the repository-scale model cannot represent differences in temperature and saturation behavior within (1) the pillars (i.e., the rock separating neighboring emplacement drifts), (2) the emplacement drifts, or (3) the waste packages (WPs) themselves. The drift-scale model is a two-dimen-

sional cross-sectional model that explicitly represents the details of the WPs and emplacement drifts in the plane orthogonal to the drift axes. This model is useful in representing details of thermo-hydrological behavior at the drift (or sub-repository) scale. In particular, we are interested in how sub-repository-scale, buoyant, gas-phase convection (which is driven by temperature differences between the drifts and pillars) affects vapor and condensate flow and thermal performance. To take advantage of symmetry, the drift-scale model assumes an infinite repository with uniformly spaced emplacement drifts. The assumption of an infinite repository area is applicable to the interior of the repository, which is not affected by cooling at the edge. This region includes most of the repository area during (at least) the first 1000 yr.

The drift-scale model assumes the 38.4-m center-to-center spacing between emplacement drifts that is found in the SCP-CDR.[15] The model represents a symmetry element from the symmetry plane down the center of the WP to the symmetry plane in the pillar between neighboring drifts. The thermal load is axially averaged along the axis of the drift. The WP has a cross section of 1.6 × 1.6 m and is located in the center of an emplacement drift that is 4.8 m high by 6.0 m wide. The drifts are assumed to remain open; therefore, heat flow from the WP surface to the drift wall occurs as thermal radiation, convection, and conduction. The drift-scale model can represent heterogeneity that occurs at the scale of the drifts. For some of our calculations, a 1.6-m-wide, high-k_b zone is oriented vertically, intersecting either the midline of the emplacement drift or the midline of the pillar separating the drifts. The k_b of this zone can be several orders of magnitude larger than k_b throughout the rest of the model (the nominal-k_b zone). The center-to-center spacing between the high-k_b zones is 38.4 m (the same as the center-to-center drift spacing).

Heterogeneity that occurs at a larger scale is represented by a third model, which we call the cross-sectional uniform heat flow (CSUHF) model. Like the drift-scale model, the CSUHF model assumes an infinite repository, thereby enabling it to take advantage of symmetry. The CSUHF model represents an infinite series of vertical, uniformly spaced, 1.0-m-wide, high-k_b zones. We considered high-k_b zone spacings of 100 and 1000 m. For the high-k_b zones, we considered 10, 84, 414, and 840 darcy. For the nominal-k_b zones, we considered 1.9 and 100 microdarcy; 1, 10, 100, and 280 millidarcy; and 10 darcy.

III. Discussion of Model Results

The following sections discuss the mountain-scale and sub-repository-scale thermo-hydrological phenomena that are summarized in Fig. 1 and Table I. In addition to the effects listed in Table I, gas-phase diffusion of air and water vapor may play an important role in large- and small-scale movement of water vapor.[16] Sections III.A discusses mountain-scale phenomena, while Section III.B addresses the impact of layered heterogeneity on that phenomena. Section III.C summarizes the influence of sub-repository-scale, buoyant, gas-phase flow. Section III.D addresses gas-phase diffusion, while Section III.E examines the potential role of heterogeneity on focusing vapor and condensate flow. Section III.F discusses the use of hypothesis testing in model validation.

III.A Mountain-Scale Boiling and Buoyant, Gas-Phase Flow

If the bulk permeability, k_b, of the fractured rock mass is sufficiently large, repository heat can lead to the development of large-scale, buoyant convection cells transporting water vapor from regions below the repository to regions above. These cells also have the potential to redistribute heat within the mountain and cool repository temperatures. We conducted a mathematical analysis[17] and a numerical modeling study[8] to determine the conditions under which these effects may be significant.

Mountain-scale, buoyant, gas-phase convection occurs within fracture networks having a connectivity with length scale comparable to the UZ thickness and repository width (Fig. 1b). For the modeling study we used the repository-scale, UZ-SZ model, and considered a wide range of k_b values and AMLs, including 27.1, 49.2 (the reference SCP-CDR thermal load), and 154.7 MTU/acre. We analyzed these effects for (1) a homogeneous and isotropic k_b distribution, and (2) a layered, heterogeneous k_b distribution. Because the matrix permeability is so small for most of the UZ, differences in k_b reflect differences in fracture permeability. We start with a discussion of the mathematical analysis.

As repository heat propagates into the rock, a column of warmer, less-dense gas develops that encompasses the repository area (Fig. 1b). The result is that gas-phase pressures, especially those at the lowest portion of the column, are lowered relative to those at the same depth in the cooler, denser column of gas outside the repository footprint. Consequently, gas from outside the repository footprint is drawn into the region below the repository and flows upward through the repository, in a fashion similar to the updraft in a chimney. Buoyant, gas-phase convection cells develop as the warmer, less-dense column of gas within the repository footprint is displaced by the cooler, denser gas from outside the repository footprint. As the initially cooler gas is heated up, its relative humidity is lowered, causing it to evaporate water from the rock matrix below the repository. This warm moist air is convected upward to where it cools above the repository, generating condensate that drains down fractures back toward the repository and/or is imbibed by the matrix, causing a

saturation buildup above the repository. Because water removed below the repository may be replenished by water imbibed from the SZ, this process can result in a net buildup of liquid water in the UZ. For large enough k_b, mountain-scale, buoyant, vapor flow can dominate moisture movement on the order of 100,000 yr (Table I).

Under sub-boiling conditions, this phenomenon always occurs and is significant unless the k_b is very small. Under boiling conditions, steam generation causes a gas pressure buildup that can dominate the buoyancy forces, thereby suppressing large-scale buoyant convection cells. For either large k_b, or as boiling diminishes, the gas pressure buildup may not be sufficient to suppress buoyancy, and convection cells form. As these cells develop, they can transport steam (or moist air) from below the repository to the condensation zone above.

For buoyant convection cells to dominate over the boiling-generated, gas-phase pressure buildup, k_b must be larger than a threshold bulk permeability, $k_b > k_b^{hyd}$, where k_b^{hyd} is given by

$$k_b^{hyd} = \frac{q_H}{h_{fg}\rho_s}\,\frac{L_b}{L}\,\frac{T_{amb}}{\Delta T_{av}}\,\frac{\mu_g}{\rho_{g,amb}g} \qquad (4)$$

where

- q_H is the instantaneous areal heat load (W/m^2),
- h_{fg} is latent heat of vaporization (J/kg),
- ρ_s is steam density (kg/m^3),
- $\rho_{g,amb}$ is mean gas-phase density under ambient conditions (kg/m^3),
- L_b is thickness of the boiling zone around the repository (m),
- L is thickness of the thermally perturbed zone (m),
- T_{amb} is the mean ambient unsaturated zone temperature (K),
- ΔT_{av} is the mean vertical change in temperature from ambient (K),
- μ_g is gas-phase viscosity (kg/m-s), and
- g is gravity acceleration (m^2/s).

Large-scale, buoyant convection cells will cool repository temperatures when gas-phase convective heat flow through the repository domain is significant compared to the areally averaged heat load. This condition occurs when k_b is sufficiently large, that is, $k_b > k_b^{th}$ where the threshold bulk permeability, k_b^{th}, is given by

$$k_b^{th} = \frac{q_H}{h_g\rho_g}\,\frac{T_{amb}}{\Delta T_{av}}\,\frac{\mu_g}{\rho_{g,amb}g} \qquad (5)$$

Here, h_g is specific enthalpy of the gas phase (J/kg), and ρ_g is the gas-phase density (kg/m^3). Because q_H is a function of time, the threshold permeabilities are functions of time. Effective values of q_H, averaged over time, should be applied in making estimates of k_b^{hyd} and k_b^{th}.

We note, in both cases, that the critical bulk permeabilities, k_b^{hyd} and k_b^{th}, are proportional to the repository heat load, q_H, and inversely proportional to the average increase in temperature, ΔT_{av}. The latter term depends on q_H and is approximately proportional to q_H under sub-boiling conditions so that increasing q_H only weakly affects k_b^{th}. Therefore, under sub-boiling conditions, the likelihood of buoyant, gas-phase convection impacting repository temperatures is relatively insensitive to AML. Note that k_b^{hyd} is not applicable to sub-boiling conditions. Under above-boiling conditions, the term ΔT_{av} depends weakly on q_H because most of the energy goes toward latent heat of boiling. Therefore, under boiling conditions, the critical bulk permeabilities, k_b^{hyd} and k_b^{th}, are approximately proportional to q_H. Consequently, higher AMLs reduce the likelihood of the impact of buoyant, gas-phase convection cells by increasing the critical bulk permeabilities for both moisture and thermal transport.

It is also important to note that because $\rho_s h_{fg} \approx \rho_g h_g$, the following approximate relationship holds:

$$k_b^{hyd} \approx \frac{L_b}{L}\,k_b^{th} \qquad (6)$$

and, therefore,

$$k_b^{hyd} < k_b^{th} \qquad (7)$$

Values of k_b that are large enough for large-scale, buoyant convection to affect repository temperatures will also be large enough to affect the large-scale movement of water vapor produced by boiling. Conversely, if k_b is small enough for the large-scale movement of water vapor to be negligible, then large-scale, buoyant convection cells will not be significant enough to cool repository temperatures. Although this method of analysis is approximate, it gives a good order-of-magnitude estimate of critical bulk permeabilities that have been verified by numerical simulations.

As an example, we consider a repository with q_H = 14.1 W/m^2, which is equivalent to an APD of 57 kW/acre. We use T_{amb} = 300 K and ΔT_{av} = 50 K. Values for ρ_s, h_g, and h_{fg} were taken at conditions for saturated water vapor at a temperature of 95°C. The values for the lengths were L = 400 m and L_b = 20 m. We then obtain k_b^{hyd} = 0.7 darcy, and k_b^{th} = 14 darcy.

Ref. 8 reports our observation that mountain-scale, buoyant, gas-phase convection does not influence temperatures at the repository center until after they peak.

Depending on the AML and k_b, the cooling effect of mountain-scale, buoyant, gas-phase convection can substantially reduce the duration of the boiling period, t_{bp}, in the repository. Depending on the proximity to the outer edge of the repository, edge cooling can also substantially reduce t_{bp}. Ref. 18 gives the details of how these cooling effects influence t_{bp} throughout the repository.

Figure 3 shows the area-weighted boiling period duration, $\bar{t}_{bp}$, as a function of k_b for the 49.2- and 154.7-MTU/acre cases. Because $\bar{t}_{bp}$ is the boiling period duration averaged over the entire repository area, and the repository-scale model assumes a uniform AML, $\bar{t}_{bp}$ effectively represents an "average" WP location. For $k_b < k_b^{th}$, $\bar{t}_{bp}$ is insensitive to k_b. For an AML of 154.7 MTU/acre, k_b^{th} is about 5 darcy, while for 49.2 MTU/acre, it is about 1 darcy. For $k_b > k_b^{th}$, $\bar{t}_{bp}$ decreases with increasing k_b. The cooling effect of mountain-scale, buoyant, gas-phase convection increases with proximity to the edge of the repository.

Relative to the 1-millidarcy case, increasing k_b to 1 darcy only reduces $\bar{t}_{bp}$ by 2.4% for an AML of 154.7 MTU/acre, while for 49.2 MTU/acre, it is reduced by 19.7% (Fig. 3). Increasing k_b to 5 darcy reduces $\bar{t}_{bp}$ by 11.4% for an AML of 154.7 MTU/acre, while for 49.2 MTU/acre, the reduction is 48.9%. Consistent with Equation (5), boiling behavior for the 49.2-MTU/acre repository was found to be more sensitive to mountain-scale, buoyant, gas-phase convection than for the 154.7-MTU/acre repository. The boiling-generated, gas-phase pressure buildup increases with AML, and it opposes the tendency for thermal buoyancy for some period of time.[8]

We compared the net buildup of liquid water above the repository, ΔV_l, for all of the thermal loads and k_b cases considered (Fig. 4). For an AML of 27.1 MTU/acre and k_b < 280 millidarcy, mountain-scale, buoyant, gas-phase convection results in a very small net change to the liquid saturation distribution (Fig. 4b); however, significant refluxing occurs, with buoyant vapor flow being balanced by condensate drainage and imbibition. For k_b > 280 millidarcy, condensate drainage and imbibition cannot keep up with buoyant vapor flow, and regions of net dryout below the repository and condensate buildup above develop and persist for tens of thousands of years. With the ECM, we cannot determine whether the resulting condensate flux results in nonequilibrium fracture flow down to the repository horizon (and possibly down to the water table). However, the potential for nonequilibrium condensate drainage exists even for situations that do not result in a net redistribution of liquid saturation. Large-scale *in situ* heater tests, conducted under both sub-boiling and above-boiling conditions, are needed to determine the potential for mountain-scale, buoyant, vapor flow to drive nonequilibrium condensate drainage in the vicinity of WPs.[19,20]

Figure 3. Area-weighted duration of the boiling period as a function of bulk permeability for AMLs of 49.2 and 154.7 MTU/acre. Note that the time scales differ by a factor of 10.

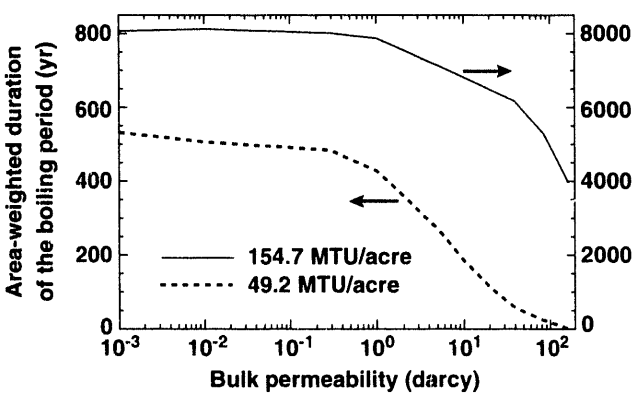

For an AML of 27.1 MTU/acre, ΔV_l increases gradually until it peaks, and declines even more gradually (Fig. 4a). A substantial ΔV_l persists well beyond 100,000 yr for the high-k_b cases. The peak ΔV_l occurs at 20,000, 20,000, 30,000, 40,000, and 40,000 yr for the 168-, 84-, 40-, 20-, and 10-darcy cases, respectively (Figs. 4a and b). For the 280-millidarcy case (Fig. 4b), the peak occurs beyond 100,000 yr. For $k_b \geq 10$ darcy, the maximum ΔV_l (called ΔV_l^{max}) increases nearly linearly with k_b. Because it cannot represent nonequilibrium fracture-matrix flow, the ECM probably underpredicts the condensate drainage flux and, consequently, may overpredict ΔV_l. However, ΔV_l is a useful indicator of the overall magnitude of condensate drainage and buildup effects. The slope of the ΔV_l vs t curve is indicative of the overall rate of condensate generation that arises from mountain-scale, buoyant, vapor flow. For high AMLs, it is indicative of the competition between vapor flow driven by the gas-pressure buildup due to boiling and vapor flow driven by thermal buoyancy.

For an AML of 49.2 MTU/acre, ΔV_l increases gradually until it peaks, and declines even more gradually (Fig. 4c). A substantial ΔV_l persists well beyond 100,000 yr for the high-k_b cases. The peak ΔV_l occurs at 20,000, 15,000, 15,000, 10,000, 6600, 5000, and 1300 yr for the 168-, 84-, 40-, 20-, 10-, 5-, and 1-darcy cases, respectively (Figs. 4c and d). For the 280- and 10-millidarcy cases, the ΔV_l occurs at 1000 yr (Fig. 4d). For AMLs of 27.1 and 49.2 MTU/acre, ΔV_l is never less than zero.

For an AML of 154.7 MTU/acre, the high-k_b cases (k_b > 5 darcy) show two peaks in the ΔV_l curve, with an early peak occurring at 300 to 500 yr and a late peak occurring beyond 20,000 yr (Fig. 4e). For the 1-darcy case, the early and late peaks occur at 900 and 20,000 yr, respectively (Fig. 4f). The early peak approximately coincides with the maximum vertical extent of boiling conditions and is related to the interaction of the heat-

pipe effect and mountain-scale, buoyant, gas-phase convection. After the initial peak, ΔV_l quickly declines for the high-k_h cases, with a trough occurring at 3000 yr, coinciding with the maximum vertical extent of dry-out. For the 40-, 84-, and 168-darcy cases, ΔV_l declines to below zero. After the trough occurs, ΔV_l resumes a gradual increase until a late peak occurs. This peak occurs at 60,000, 50,000, 50,000, and 25,000 yr for the 168-, 84-, 40-, and 5-darcy cases, respectively. For 10 millidarcy < k_h < 1 darcy, there is no early peak in ΔV_l, and a late peak occurs at 20,000 yr (Fig. 4f). For $k_h \leq 10$ millidarcy, after a brief early period with very small positive values, ΔV_l is always negative (Fig. 4f). Therefore, if the large-scale connected k_h is small enough, mountain-scale, buoyant, gas-phase convection does not result in a liquid water buildup above the repository for the 154.7-MTU/acre case.

Figure 4. Net buildup of liquid water above the repository for various values of k_h and AMLs of 27.1 MTU/acre (a and b), 49.2 MTU/acre (c and d), and 154.7 MTU/acre (e and f).

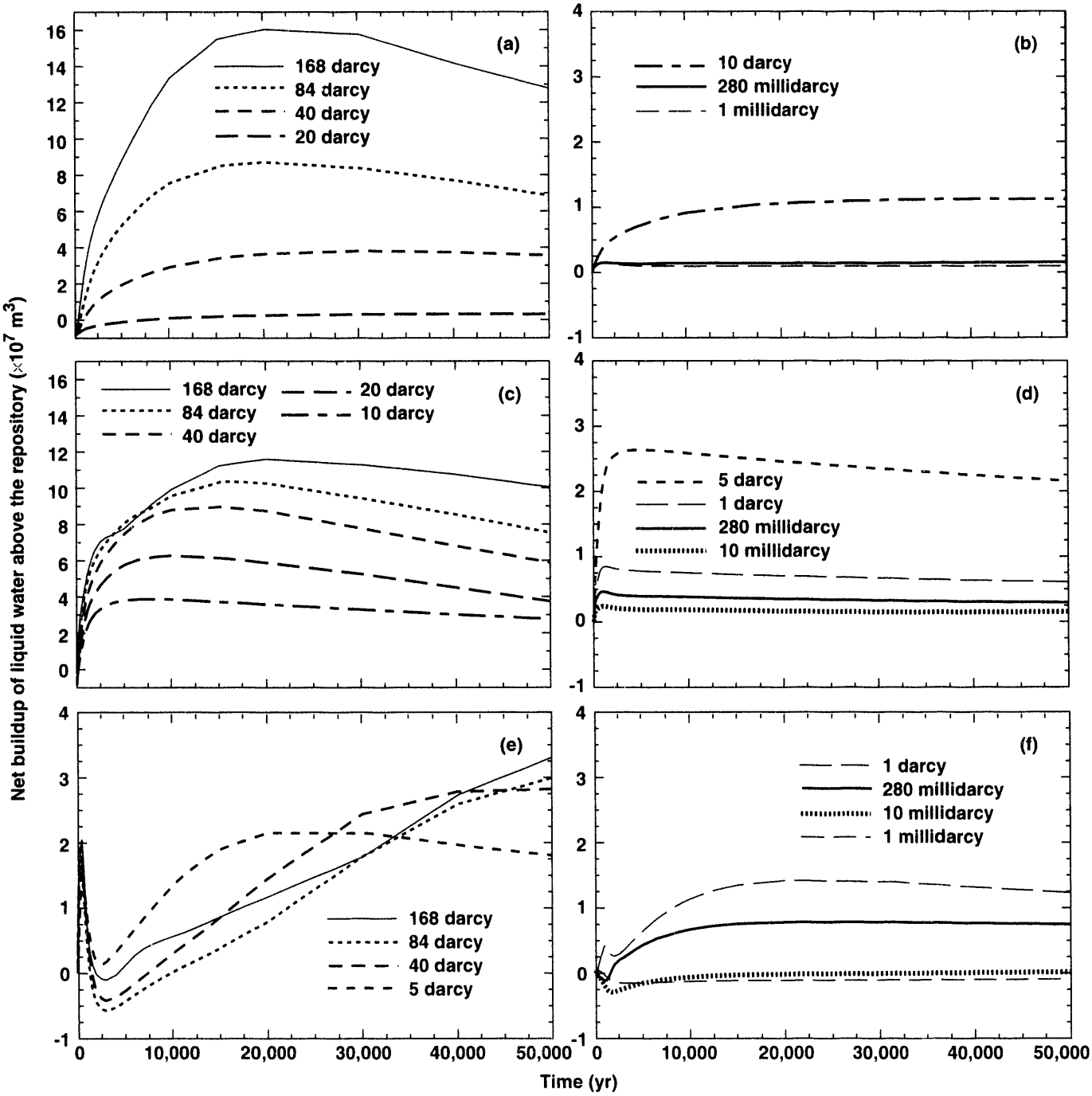

Figure 5 shows the ΔV_l^{max} as a function of k_b for AMLs of 27.1, 49.2, and 154.7 MTU/acre. Notice that the shape of this curve varies significantly among the various AML cases. For an AML of 154.7 MTU/acre, the slope of the curve is nearly constant, with ΔV_l^{max} increasing gradually with k_b. For AMLs of 27.1 and 49.2 MTU/acre, the slope is highly variable. For small k_b, the slope is very shallow. For an AML of 49.2 MTU/acre, the slope increases abruptly at k_b = 1 darcy, while for 27.1 MTU/acre, it increases abruptly at 10 darcy. Therefore, the dependence of ΔV_l^{max} on k_b is very nonlinear for AMLs of 27.1 and 49.2 MTU/acre.

Over the range of 1 millidarcy to 168 darcy, the following observations can be made from Fig. 5. For k_b < 20 millidarcy, the 154.7-MTU/acre case has the smallest ΔV_l^{max}, with the 49.2-MTU/acre case having the largest ΔV_l^{max}. For 20 < k_b < 50 millidarcy, the 49.2-MTU/acre case has the largest ΔV_l^{max}. For 50 millidarcy < k_b < 2.5 darcy, the 154.7-MTU/acre case has the largest ΔV_l^{max}. For 2.5 darcy < k_b < 100 darcy, the 49.2-MTU/acre case has the largest ΔV_l^{max}. For k_b > 100 darcy, the 27.1-MTU/acre case has the largest ΔV_l^{max}. Where the impact of mountain-scale, buoyant, gas-phase convection is greatest, low-to-intermediate AMLs result in the largest ΔV_l^{max}. For intermediate k_b (280 millidarcy to 1 darcy), where the impact of mountain-scale, buoyant, gas-phase convection is relatively moderate, ΔV_l^{max} for the various AML cases generally varies by less than a factor of 2.

It is likely that the k_b distribution at Yucca Mountain will be highly variable. Some of that variability will be random, while some may be correlated with discrete hydrological features such as fault zones or hydrostratigraphic units like the nonwelded vitric tuff units (PTn and CHnv). According to Weeks,[21] k_b at the repository horizon in the TSw2 may be 200 darcy. If the k_b distribution spans a significant fraction of the range shown in Fig. 5 (including regions in which k_b > 10 darcy), then mountain-scale hydrothermal behavior will be more variable for low-to-intermediate AMLs than for high AMLs. If the k_b distribution only spans the lower end of the k_b range (k_b < 1 darcy), then mountain-scale hydrothermal behavior will be less variable for all AMLs.

Figure 5. Maximum net buildup of liquid water above the repository as a function of bulk permeability for various AMLs.

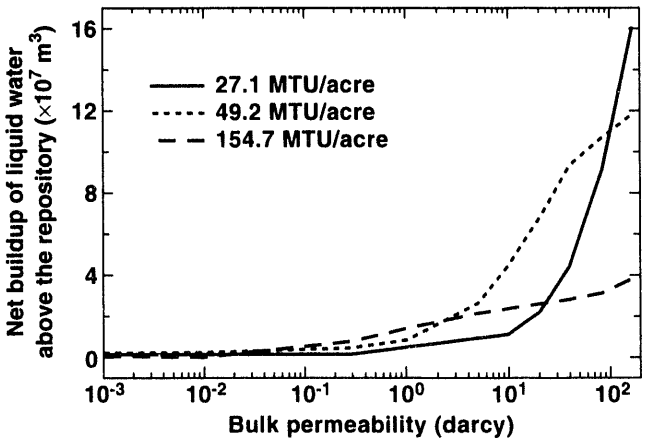

III.B Impact of Layered Heterogeneity on Mountain-Scale Phenomena

We also considered cases in which the k_b distribution varies vertically, which results in a layered heterogeneous k_b distribution. This was done in consideration of the unpublished k_b data of Weeks,[22] which indicates considerable layering of k_b. In particular, it appears that k_b may be far smaller in the nonwelded vitric units (PTn and CHnv) and the nonwelded zeolitized unit (CHnz) than in the welded units (TCw, TSw1, TSw2, and TSw3). The depth intervals of the hydrostratigrahic units are given in Table II. For AMLs of 27.1 and 154.7 MTU/acre, we considered four k_b distributions:

(1) k_b = 84 darcy everywhere.
(2) k_b = 320 millidarcy in the PTn; otherwise, k_b = 84 darcy.
(3) k_b = 280 millidarcy in the CHn; otherwise, k_b = 84 darcy.
(4) k_b = 320 millidarcy in the PTn and 280 millidarcy in the CHn; otherwise, k_b = 84 darcy.

Figure 6 shows the net buildup of liquid water above the repository, ΔV_l, for these four cases. For the 27.1-MTU/acre repository, a reduced k_b in the PTn reduces ΔV_l by half (Fig. 6a). For the uniform-k_b case, mountain-scale, buoyant, gas-phase convection behaves as though it is in an "open" system with respect to the ground surface. In this open system, the gas-phase velocity vectors are orthogonal to the ground surface in the vicinity of the ground surface. Buoyant vapor flow results in a substantial increase in liquid saturation from the repository horizon all the way to the ground surface. When k_b in the PTn is reduced, this unit functions as a gas-phase flow barrier or "vapor cap." Consequently, the direction of gas-phase flow below the PTn/TSw1 contact becomes tangential to this contact rather than crossing it. The PTn effectively isolates the buoyant, gas-phase, convection cells from the ground surface, thereby causing the convective system to be "closed" with respect to the ground surface. The resulting decrease in the gas-phase flow velocities causes an overall reduction in ΔV_l (Fig. 6a).

For the 154.7-MTU/acre repository, a reduced k_b in the PTn has a much different effect on ΔV_l (Fig. 6b). As in the 27.1-MTU/acre case, the reduced k_b in the PTn causes the buoyant convective system to be closed with

respect to the ground surface, reducing the magnitude of gas-phase flow. The resulting decrease in the gas-phase flow velocities reduces the initial peak in ΔV_l by 40% (Fig. 6b). Recall that for the high-k_h cases (Fig. 4e), we observed an initial peak in ΔV_l at about 300 to 500 yr, followed by a steep decline (and trough) in the ΔV_l curve. The steep decline arises from buoyant convection driving water vapor to the ground surface. Figure 6b clearly indicates that an open convective system driven by a high-AML repository results in a substantial loss of water vapor to the atmosphere. However, an open convective system driven by a low-AML repository does not result in such a loss. The key difference is that boiling in the high-AML case drives most of the moisture buildup to the upper 100 m of the unsaturated zone (UZ), while for the low-AML case, the moisture buildup is spread over the upper 340 m of the UZ. Proximity of the moisture buildup to the ground surface, and larger gas-phase velocities, facilitates the loss of moisture to the atmosphere for the high-AML case. When the PTn acts as a vapor cap, the loss of moisture to the atmosphere is impeded, trapping much of the moisture convected to upper UZ. Consequently, the trough in the ΔV_l curve is less pronounced, and the following increase in ΔV_l is steeper (Fig. 6b).

For the 154.7-MTU/acre repository, the reduced k_h in the PTn causes the second peak in the ΔV_l curve to occur much earlier (15,000 yr) than in the uniform-k_h case (50,000 yr). The earlier occurrence of the second peak is caused by the gas-phase diffusive loss of moisture to the atmosphere. Note that the value assumed for the effective diffusion factor, τ_{eff} ($\tau_{eff} = 0.2$), may be low compared to experimental values measured by soil physicists (see Section III.D). A larger value of τ_{eff} would result in a larger diffusive loss of moisture to the atmosphere and an overall reduction in ΔV_l.

For the 27.1-MTU/acre repository, a reduced k_h in the CHn reduces ΔV_l by half, which is almost identical to the effect that a reduced-k_h PTn has on ΔV_l (Fig. 6a). The reduction in k_h in the CHn impedes buoyant flow through it, effectively decoupling it from from the mountain-scale, buoyant convective system. The resulting reduction in the vertical extent of the buoyant convective system has the effect of reducing the gas-phase velocities and the quantity of water that can be vaporized and convected from below the repository to above, where it condenses. Reducing k_h in both the PTn and CHn reduces ΔV_l by another factor of 2 relative to the case with the reduced k_h in the PTn (Fig. 6a).

For the 154.7-MTU/acre repository, a reduced k_h in the CHn reduces ΔV_l by nearly half (Fig. 6b), which is

Figure 6. Net buildup of liquid water above the repository for various vertical k_h distributions and AMLs of (a) 27.1, and (b) 154.7 MTU/acre. Uniform k_h = 84 darcy. The value of k_h in the PTn is reduced to 320 millidarcy, and in the CHn, to 280 millidarcy.

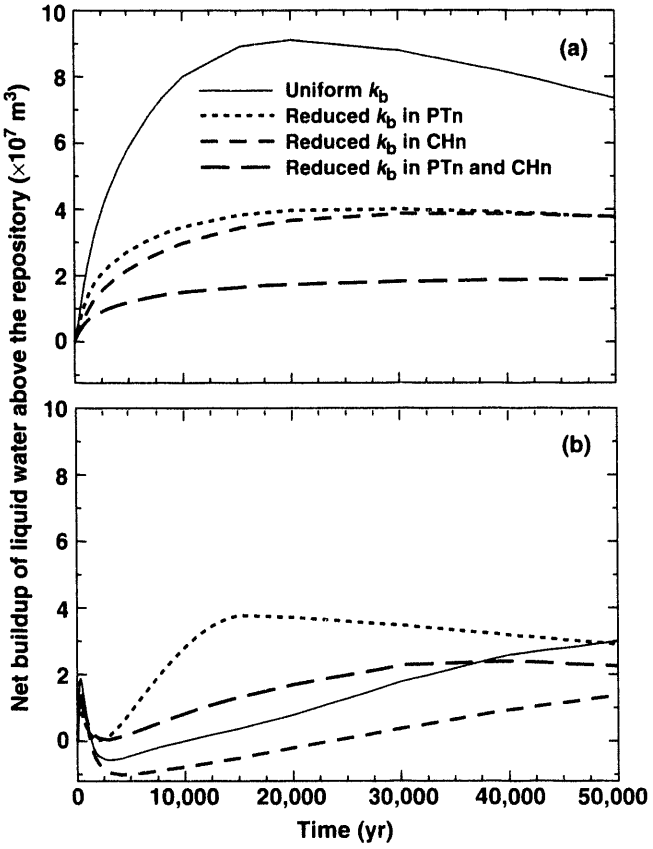

Figure 7. Duration of the boiling period at various repository locations for various vertical k_h distributions and an AML of 154.7 MTU/acre. Uniform k_h = 84 darcy. The value of k_h in the PTn is reduced to 320 millidarcy, and in the CHn, to 280 millidarcy. The repository locations are identified as the percentage of the repository area enclosed, with 0% corresponding to the repository center, and 100% corresponding to the outer perimeter.

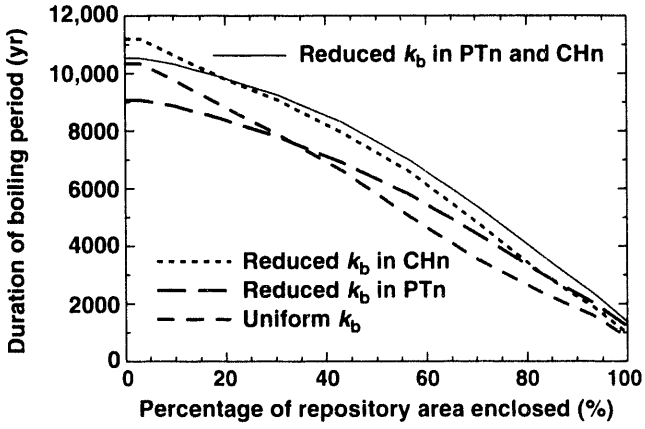

similar to the effect shown for the 27.1-MTU/acre repository (Fig. 6a). Reducing k_b in both the PTn and CHn reduces ΔV_l by nearly half relative to the case with the reduced k_b in the PTn (Fig. 6a). Figure 7 shows the impact that a reduced k_b in the PTn and CHn has on the boiling period duration, t_{bp}. The reduction in gas-phase velocities decreases the overall convective cooling effect, thereby increasing t_{bp}, particularly at the outer repository area.

III.C Sub-Repository-Scale, Boiling and Buoyant, Gas-Phase Flow

Sub-repository-scale, buoyant, gas-phase convection occurs within fracture networks having a connectivity with length-scale comparable to the distance between the hot and cold regions of the repository (Fig. 1a). Buoyant, gas-phase convection cells develop as the warmer, less-dense column of gas within the footprint of the waste packages (WPs) is displaced by the cooler, denser column of gas in the adjacent areas. As the initially cooler gas is heated up, its relative humidity is lowered, causing it to evaporate water from the rock matrix below hot regions of the repository. This warm moist air is convected upward to where it cools above the WPs. This generates condensate that drains down fractures back toward the repository and/or is imbibed by the matrix, causing a saturation buildup above the WPs. High AMLs result in a large zone of above-boiling temperatures, which suppresses the effects of sub-repository-scale, buoyant vapor flow.[8] Sub-repository-scale, buoyant, gas-phase convection continues as long as significant temperature differences persist within the repository. We find that it can dominate moisture movement for up to 1000 yr for the drift spacing described in the Site Characterization Plan–Conceptual Design Report (SCP–CDR).[15]

More recently, there has been considerable momentum toward the use of the multi-purpose container (MPC), which, compared with the WP described in the SCP–CDR, is much larger, contains more fuel assemblies, and therefore has a higher thermal output per WP. The larger drift spacing, which is consistent with the use of larger WPs, will result in temperature differences within the repository persisting longer. Consequently, the effects of sub-repository-scale, buoyant vapor flow will also be more persistent, possibly lasting thousands of years.[18] If, as Weeks[21] suggests, k_b at the repository horizon is found to be on the order of 200 darcy, the impact of sub-repository-scale, buoyant, gas-phase convection will be extremely significant.

Ref. 18 analyzes sub-repository-scale performance for large WPs containing either 21 PWR or 40 BWR spent nuclear fuel (SNF) assemblies with a center-to-center WP spacing of 12 m. These calculations also apply to a 12-PWR/21-BWR SNF emplacement scenario with a center-to-center WP spacing of 6.86 m. An important observation from that study concerns the substantial difference between thermo-hydrological performance predicted by repository-scale models and that predicted by drift-scale models. For an AML of 24.2 MTU/acre, the repository-scale model predicts a peak temperature, T_{peak}, of 65°C, while the drift-scale model predicts T_{peak} of up to 172°C on the WP surface and 144°C in the rock adjacent the drift. While the repository-scale model predicts no boiling period, the drift-scale model predicts a boiling period duration, t_{bp}, of 183 to 202 yr in the rock and 300 to 350 yr on the WP surface. Similarly, the repository-scale model predicts no boiling period for an AML of 35.9 MTU/acre, while the drift-scale model predicts t_{bp} of 955 to 1014 yr in the rock and 1111 to 1155 yr on the WP surface.

Another important observation about sub-repository-scale performance is that T_{peak} varies modestly for AMLs ranging from 24.2 to 55.3 MTU/acre.[18] Because it occurs so early (12 to 25 yr), T_{peak} is insensitive to whether the distance to the adjacent emplacement drift is 43.4 m or 99.0 m. For the high-AML cases, the drift spacing is small enough to cause T_{peak} to be sensitive to drift spacing. Consequently, T_{peak} is significantly greater for the 110.5-MTU/acre case than for the 83.4-MTU/acre case.[18]

Another important observation is that t_{bp} is insensitive to sub-repository-scale, buoyant, gas-phase convection for both the low- and high-AML cases (24.2, 35.9, and 110.5 MTU/acre). For intermediate-AML cases (55.3 and 83.4 MTU/acre), t_{bp} is modestly sensitive. For high AMLs, the extent of dry-out is insensitive to sub-repository-scale, buoyant, gas-phase convection. For low AMLs, the extent of moisture movement (i.e., dry-out and condensate buildup) is very dependent on the magnitude of sub-repository-scale, buoyant, gas-phase convection.

Some have equated the term "sub-boiling repository" with a repository system for which the hydrological impact of heat is insignificant. Some also define a "sub-boiling repository" to be one in which the average repository temperature is below the boiling point. Our analyses show that boiling conditions can persist around an emplacement drift even if the average repository temperature is well below boiling. Moreover, if buoyant, gas-phase convection is found to be significant, it can drive substantial vapor and condensate fluxes whether or not boiling ever occurs. On the other hand, if buoyant, gas-phase convection is found to be insignificant, a boiling period of sufficiently limited duration may be shown to generate condensate fluxes that have a minor impact on waste package performance and radionuclide transport. The absence of local boiling conditions is not, in itself, an adequate indicator of whether repository heat drives significant vapor and condensate flow. Average repository temperatures are an even poorer indicator of whether repository-heat-driven hydrothermal flow significantly impacts the performance of a low-AML repository.

Diagnosing whether sub-boiling conditions can be equated with the absence of significant repository-heat-driven effects will require *in situ* heater tests conducted under sub-boiling as well as above-boiling conditions.[19,20]

III.D Gas-Phase Diffusion of Water Vapor

Transport of water vapor in the gas phase takes place by two mechanisms: (1) advective transport from movement of the gas phase, and (2) diffusive transport by the process of molecular diffusion. The binary diffusive mass flux of a component in a gas phase is governed by Fick's law, which for a porous medium takes the form

$$q = -\phi S_g \rho_g \tau \eta D \nabla \omega \qquad (8)$$

where ϕ is porosity, S_g is gas-phase saturation, ρ_g is gas density, τ is the tortuosity factor, η is the diffusion enhancement factor, D is the binary diffusion coefficient, and ω is the mass fraction of the component. The tortuosity factor, τ, is the reciprocal of the tortuosity and takes into account the increased path length within the porous medium. Its value is always less than or equal to unity.

The diffusion enhancement factor, η, which appears in Equation (8), can be taken to be unity for a noncondensible component or isothermal conditions. For diffusion of a condensible component, such as water vapor, driven by a thermal gradient, the diffusive flux is enhanced, so that η is greater than unity. The well-known paper by Philip and de Vries[23] gives an explanation for this enhancement. Normally, diffusive transport of water vapor is obstructed by liquid water that blocks pore throats; consequently, diffusion is reduced at higher liquid saturations. However, the thermal gradient sets up a vapor pressure gradient in the gas phase which causes water to evaporate from a blockage and diffuse in the gas phase to a cooler blockage, where it condenses. The process continues as the water evaporates on the other side of the blockage. The mechanism whereby liquid water flows through a blockage is the pressure difference caused by the difference in meniscus curvature between the two sides.

Another phenomenon further increases diffusive fluxes under nonisothermal conditions. The gas-phase thermal conductivity is much less than that in the liquid and solid phases, so that the temperature gradient in the gas phase between liquid blockages is greater than the average temperature gradient of the bulk porous medium. The resulting increase in water vapor concentration gradients within the gas phase further increases diffusive fluxes compared to isothermal systems.

The diffusion enhancement factor is a function of liquid saturation and appears to increase significantly at sufficiently large saturations when blockages can occur, which is consistent with the above theory. The diffusion enhancement factor, η, appears to have been measured only for soils. Cass and others[24] obtained values of η for sand that ranged from unity at 0% liquid saturation (i.e., no enhancement) to 12 at 80% liquid saturation. The value of η appears to decrease with increasing temperature. The maximum value of η decreased by almost 50% as temperature was increased from 3.5 to 32.5°C. This trend can be explained by the theory of Philip and de Vries. At greater temperatures, the higher latent heat carried by diffusive transport enhances heat transfer across the gas phase between blockages. The resulting decrease in gas-phase temperature gradients reduces the vapor-pressure gradients that drive diffusive transport.

The values of η are not directly input to the V-TOUGH code. Instead, V-TOUGH requires an effective gas-phase diffusion factor, τ_{eff}, which combines η with the tortuosity factor, τ, as follows:

$$\tau_{eff} = \eta\tau \qquad (9)$$

V-TOUGH treats τ_{eff} as a constant. If we take τ to be 0.2, and consider the upper value of 12 measured for η by Cass, we would get a value of 2.4 for τ_{eff}. For the 154.7-MTU/acre, 280-millidarcy case, we considered three values of τ_{eff}: 0.2, 1, and 2, which nearly span the range that may be applicable to this problem. Note that, unless specified otherwise, our calculations assume a value of 0.2 for τ_{eff}. Increasing τ_{eff} from 0.2 to 1 (thereby increasing gas-phase diffusion) results in a minor cooling effect (Fig. 8a). This cooling effect, which arises because of the increased transport of latent heat away from the repository, reduces the area-weighted boiling period duration, $\bar{t}_{bp}$, from 7984 to 7622 yr. Increasing τ_{eff} from 0.2 to 1 also has a minor drying effect, modestly reducing the net buildup of liquid water above the repository, ΔV_l (Fig. 8c). The maximum value of ΔV_l is only reduced by 3.2%.

As in past studies,[7,8] when analyzing dry-out and re-wetting behavior, we use the term, normalized liquid saturation, $\bar{S}_l$, which is given by

$$\bar{S}_l = \frac{S_l}{S_{l,init}} \qquad (10)$$

where S_l is the current liquid saturation, and $S_{l,init}$ is the initial (or ambient) liquid saturation. In Ref. 18 we examine the re-wetting behavior of various AMLs by comparing the duration of time that S_l in the repository is below 90% of ambient as a function of repository location. Because $\bar{S}_l = 0.9$ when S_l has been restored to 90% of ambient, we call this time $t(\bar{S}_l = 0.9)$. The area-weighted value of $t(\bar{S}_l = 0.9)$ for the entire repository is called $\bar{t}(\bar{S}_l = 0.9)$, which is essentially the mean re-wetting time for the repository.

Figure 8b utilizes $t(\bar{S}_l = 0.9)$ to illustrate re-wetting behavior as a function of repository location for a range of τ_{eff}. Notice that the drying effect that results from enhanced gas-phase diffusion of water vapor increases the duration of time that most of the repository is below ambient saturation. For the inner 25% of the repository, $t(\bar{S}_l = 0.9)$ is reduced somewhat (Fig. 8b) because of the reduction of t_{bp} (Fig. 8a). Because temperatures decrease with vertical distance from the repository horizon, gas-phase diffusion drives water vapor vertically away from the repository. Because temperatures also decrease with increasing radial distance, gas-phase diffusion also drives water vapor radially away from the repository. Notice that the enhanced dry-out effect is greatest at the outer repository area, where temperature gradients drive water vapor radially as well as vertically away from the repository. Increasing τ_{eff} from 0.2 to 1 has the effect of increasing $t(\bar{S}_l = 0.9)$ for the outer 75% of the repository. Consequently, $\bar{t}(\bar{S}_l = 0.9)$ is increased from 63,436 to 68,721 yr for the entire repository.

Figure 8. Duration of the boiling period (a) and duration of time below 90% of ambient liquid saturation (b) at various repository locations for an AML of 154.7 MTU/acre, k_h = 280 darcy, and various values of the effective diffusion factor, τ_{eff}. The repository locations are identified as the percentage of the repository area enclosed, with 0% corresponding to the repository center, and 100% corresponding to the outer perimeter. (c) The net buildup of liquid water above the repository is also plotted for these cases.

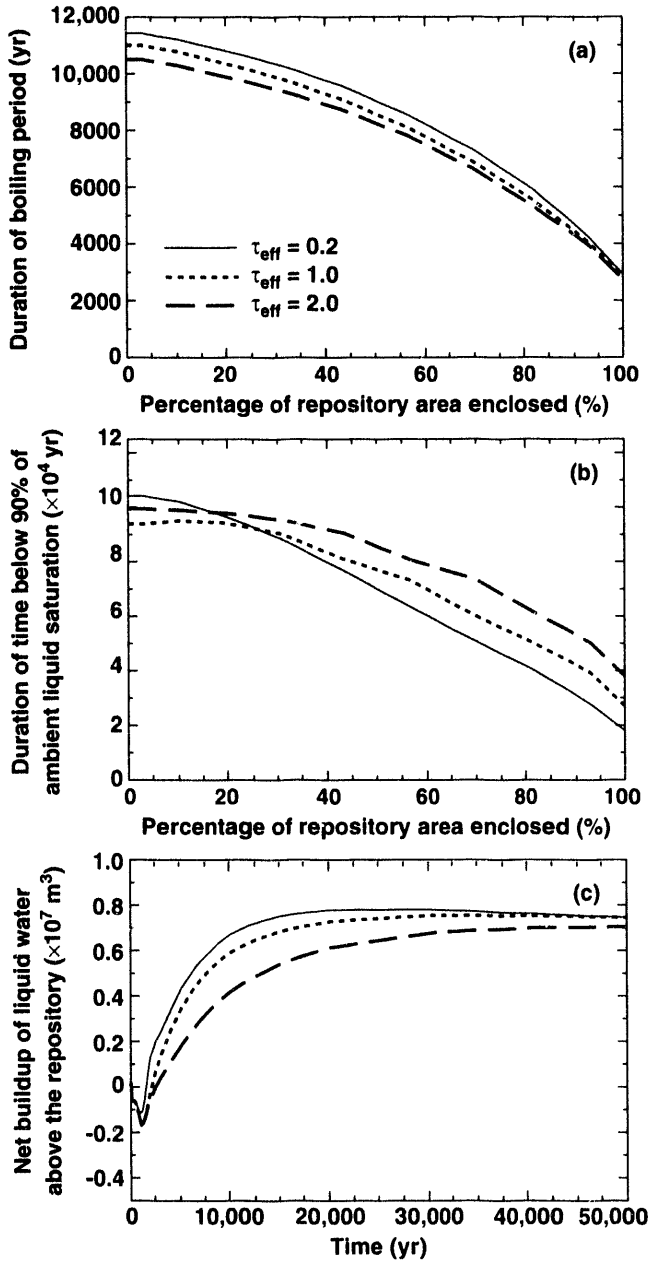

Increasing τ_{eff} from 0.2 to 2 results in a more substantial cooling effect, reducing $\bar{t}_{bp}$ from 7984 to 7323 yr (Fig. 8a). The greatest cooling effect occurs at the repository center (where the highest temperatures occur) and decreases with increasing distance from the repository center. At the repository edge, the cooling effect is minor. Increasing τ_{eff} from 0.2 to 2 also has a drying effect, reducing the maximum value of ΔV_l by 9.7% (Fig. 8c). The drying effect also increases $t(\bar{S}_l = 0.9)$ for the outer 80% of the repository (Fig. 8b). Consequently, $\bar{t}(\bar{S}_l = 0.9)$ is increased from 63,436 to 77,423 yr for the entire repository. In general, for the range of τ_{eff} considered, enhanced gas-phase diffusion results in a minor cooling effect and a minor drying effect. We plan to consider larger values of τ_{eff} and a larger range of AMLs in examining the influence of enhanced gas-phase diffusion.

The issue has been raised concerning the role that enhanced gas-phase diffusion might play in transporting water vapor from the water table to the repository at late time. As shown below, this late time occurs well after temperatures have dropped below boiling. Because gas-phase diffusion is primarily driven by temperature gradients, it is useful to plot the temperature difference between the top of the saturated zone (SZ) and the repository horizon (Fig. 9). Because the repository is the primary source of heat flow for a long period of time, temperatures at the repository exceed those at the top of the SZ for a long period of time. As long as this occurs, the diffusive flux of water vapor below the repository will be downward (away from the repository). Eventually, the geothermal flux will again dominate the vertical temperature profile, causing it to be reversed (i.e., directed from the SZ back toward the repository). Figures 9a and b show this effect for AMLs of 27.1 and 154.7 MTU/acre. For an AML of 27.1 MTU/acre, it takes 3000 yr before the vertical temperature gradient reverses at the outer edge of the repository, and 5850 yr at the repository center (Fig. 9a).

For an AML of 154.7 MTU/acre, it takes 20,400 yr before the temperature gradient reverses at the outer edge of the repository, and 34,400 yr at the repository center (Fig. 9b). Consequently, the diffusive flux of water vapor from the SZ will be directed up toward a low-AML repository long before it is for a high-AML repository. Figures 9a and b show that the vertical temperature gradients that drive water vapor from the SZ to the repository (1) are steeper, (2) occur over a greater percentage of the repository area, and (3) last longer for the 27.1-MTU/acre case than for the 154.7-MTU/acre case. Therefore, the contribution of the diffusive flux of water vapor from the SZ to the overall moisture balance at the repository will be greater for low AMLs than for high AMLs.

Figure 9. Temperature difference between the top of the saturated zone (SZ) and the repository horizon at various radial positions for k_h = 280 millidarcy. Curves are plotted for (a) an AML of 27.1 MTU/acre, and (b) an AML of 154.7 MTU/acre. Note that a positive temperature difference corresponds to the temperature at the top of the SZ being greater than that at the repository horizon. The radial positions are identified as the percentage of the repository area enclosed, with 0% corresponding to the repository center, and 100% corresponding to the outer perimeter.

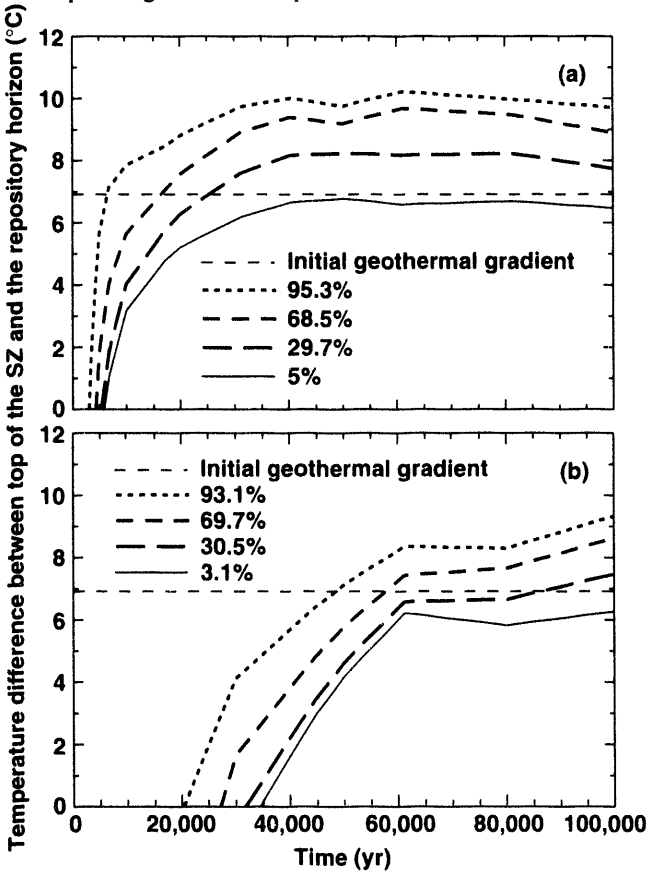

In considering the potential significance of enhanced vapor diffusion in transporting water vapor from the SZ, it is useful to compare the repository-heat-driven temperature gradients with the initial geothermal gradient. At the center of the repository, the temperature gradient never exceeds the initial geothermal gradient (Figs. 9a and b). At the repository edge, the maximum temperature gradient is 45% greater than the initial geothermal gradient. Compared to the measured range in the diffusion enhancement factor, η, the range of variability for the vertical temperature gradient below the repository is negligible. In considering the impact of enhanced vapor diffusion on the repository moisture balance at late time, it is important to note that not only is water vapor diffusing up from below the repository but also away from the repository, both vertically and radially. Water vapor diffuses radially because temperatures decrease radially away from the repository, and it diffuses vertically upward because temperatures decrease with height above the repository. It should be noted that the vertical temperature gradient above the repository is always greater than the gradient below. Moreover, the vertical temperature gradient above the repository and the radial temperature gradient are greater for higher AML. These observations corroborate what was shown in Figs. 8b and c: that the net effect of enhanced vapor diffusion on the moisture balance at the repository is to make it drier rather than wetter.

III.E Focused Vapor and Condensate Flow

Refluxing, or the heat-pipe effect, is important to consider because it can affect repository performance in two ways. First, refluxing maintains local temperatures near the boiling point, making it more difficult to dry the rock out. Consequently, the relative humidity may remain high, increasing the likelihood of a liquid film on waste package (WP) surfaces. Second, refluxing can bring mobile liquid water in contact with WPs, affecting waste-form dissolution and radionuclide transport.

To investigate the impact of heterogeneity on the focusing of vapor flow and condensate drainage (and how that focusing affects the development of heat pipes), we used a cross-sectional drift-scale model and a cross-sectional uniform heat flow (CSUHF) model.[8] Both models are used to investigate the effect of lateral variability of k_h. In particular, we consider the situation in which k_h in vertically contiguous high-k_h zones is much larger than k_h throughout the rest of the fractured rock (the nominal-k_h zones). These models specifically address how focused condensate drainage might arise from gas-phase focusing. Recent analytical work by Nitao and others[25] addresses how focused condensate drainage might arise from liquid-phase focusing.

The degree of vapor flow focusing into the high-k_b zone, and the resulting duration of refluxing at the repository horizon, depends on three factors. First, k_b in the nominally fractured zone must be large enough not to significantly throttle the rate of vapor generation due to boiling (or due to evaporation under sub-boiling conditions). Second, a large contrast in k_b between the high- and nominal-k_b zones results in a gas-phase pressure differential between these zones that preferentially drives vapor flow into the high-k_b zone (Fig. 1c). If enough vapor enters and condenses in the high-k_b zone, the return condensate flux will be large enough to maintain refluxing at the repository horizon, possibly resulting in water dripping onto WPs. Third, there must be sufficient spacing between the high-k_b zones to drive enough water vapor into these zones to result in the local condensate drainage flux being substantially greater than the mean condensate flux. Effectively, the high-k_b zones are competing for a finite quantity of vapor flow and condensate generation. Consequently, there is a trade-off between the duration of refluxing and the number of locations where it can occur in the repository. If there are too many such zones, there will be insufficient condensate focusing to cause persistent refluxing at the repository horizon. The degree of focusing necessary to cause persistent refluxing limits the number of locations where it can occur. Therefore, it is unlikely that refluxing can dominate the overall thermal behavior in the repository.

Figure 10 shows the effect of focused vapor and condensate flow on the normalized liquid saturation, $\bar{S}_l$, distribution [see Eq. (10)] in the vicinity of an emplace-

Figure 10. Dimensionless liquid saturation distribution orthogonal to an emplacement drift containing 30-yr-old SNF, for an AML of 154.7 MTU/acre and an APD of 114 kW/acre. Within the 1.6-m-wide, high-k_b zone, k_b = 84 darcy; otherwise, k_b = 10 millidarcy. Distributions are shown at time t of (a) 8, (b) 30, and (c) 200 yr for a k_b distribution in which the high-k_b zone intersects the center of the emplacement drift. Distributions are also shown at time t of (d) 30, (e) 40, and (f) 200 yr for a k_b distribution in which the high-k_b zone intersects the center of the pillar separating the emplacement drifts. The medium-shaded area surrounding the drift corresponds to a region that is drier than ambient saturation (dry-out zone). The dark-shaded areas correspond to regions that are wetter than ambient saturation (condensation zones). The lighter shading surrounding the dark-shaded areas corresponds to a decreasing buildup in saturation (outer edges of condensation zones). No shading indicates no change in saturation. Note that the transition from drier to wetter conditions is shown as a white ring at early time, which becomes a white band at later time.

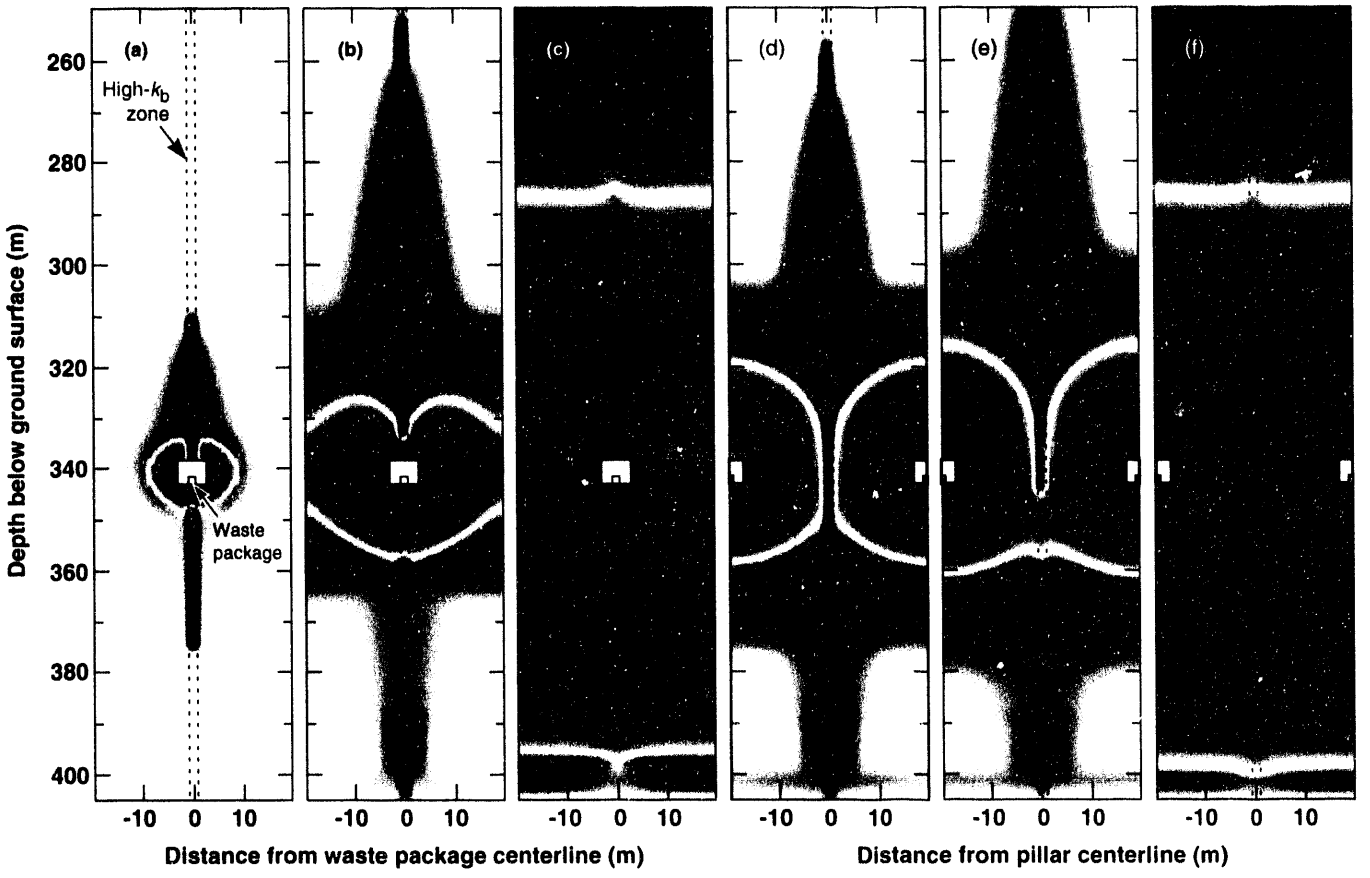

ment drift containing 30-yr-old spent nuclear fuel (SNF) with an AML of 154.7 MTU/acre for two cases of a heterogeneous k_h distribution. For both cases, 1.6-m-wide, 168-darcy, high-k_h zones alternate with 36.8-m-wide, 10-millidarcy, nominal-k_h zones. For the first case of k_h heterogeneity (Figs. 10a–c), the high-k_h zones are vertically aligned along the axis of the emplacement drifts. For the second case of k_h heterogeneity (Figs. 10d–f), the high-k_h zones are vertically aligned along the midline of the pillar separating emplacement drifts. For the first case, we also considered an AML of 49.2 MTU/acre for 10-yr-old SNF (Figs. 11a–c) and 20-yr-old SNF (Figs. 11d–e).

For the first case of k_h heterogeneity, the gas-phase pressure differential between the high- and nominal-k_h zones drives water vapor back toward the drift and into the high-k_h zone (Figs. 10a and b). Water vapor flows up the high-k_h zone until it condenses and drains back down. In effect, the emplacement drift functions as a manifold that enhances the gas-phase communication between the high- and nominal-k_h zones. If enough water vapor enters and condenses in this zone, the condensate drainage flux will be large enough to maintain refluxing in the repository. The resulting heat-pipe effect enables the temperature at the top of the drift to remain at the boiling point, causing a depression in the dry-out zone (Figs. 10a). In spite of persistent refluxing, the temperatures along most of the remainder of the drift wall, the air in the drift, and the WP itself are well above boiling. Therefore, although liquid water may be dripping in the drift, the relative humidity around the WP can still be low.

The heat-pipe zone attracts heat flow (mainly by conduction) from the neighboring, nominal-k_h rock. In effect, the heat-pipe zone functions as a "cooling fin" that is manifested by an elongated region of liquid saturation buildup (Fig. 10). The process of gas-phase focusing into the heat-pipe zone develops more quickly than the process of attracting heat from the neighboring rock. Within 8.5 yr, enough heat is being conducted into the heat-pipe zone for the 154.7-MTU/acre case to overwhelm the heat pipe, causing the top of the drift to begin to dry out. Although

Figure 11. Dimensionless liquid saturation distribution orthogonal to an emplacement drift containing SNF, for an AML of 49.2 MTU/acre. Within the 1.6-m-wide, high-k_h zone, k_h = 84 darcy; otherwise, k_h = 10 millidarcy. Distributions are shown at time t of (a) 62, (b) 663, and (c) 1000 yr for 10-yr-old SNF and an APD of 57 kW/acre. Distributions are also shown at time t of (d) 159, (e) 661, and (f) 2534 yr for 20-yr-old SNF and an APD of 43.7 kW/acre. Shading values are as described in Fig. 10.

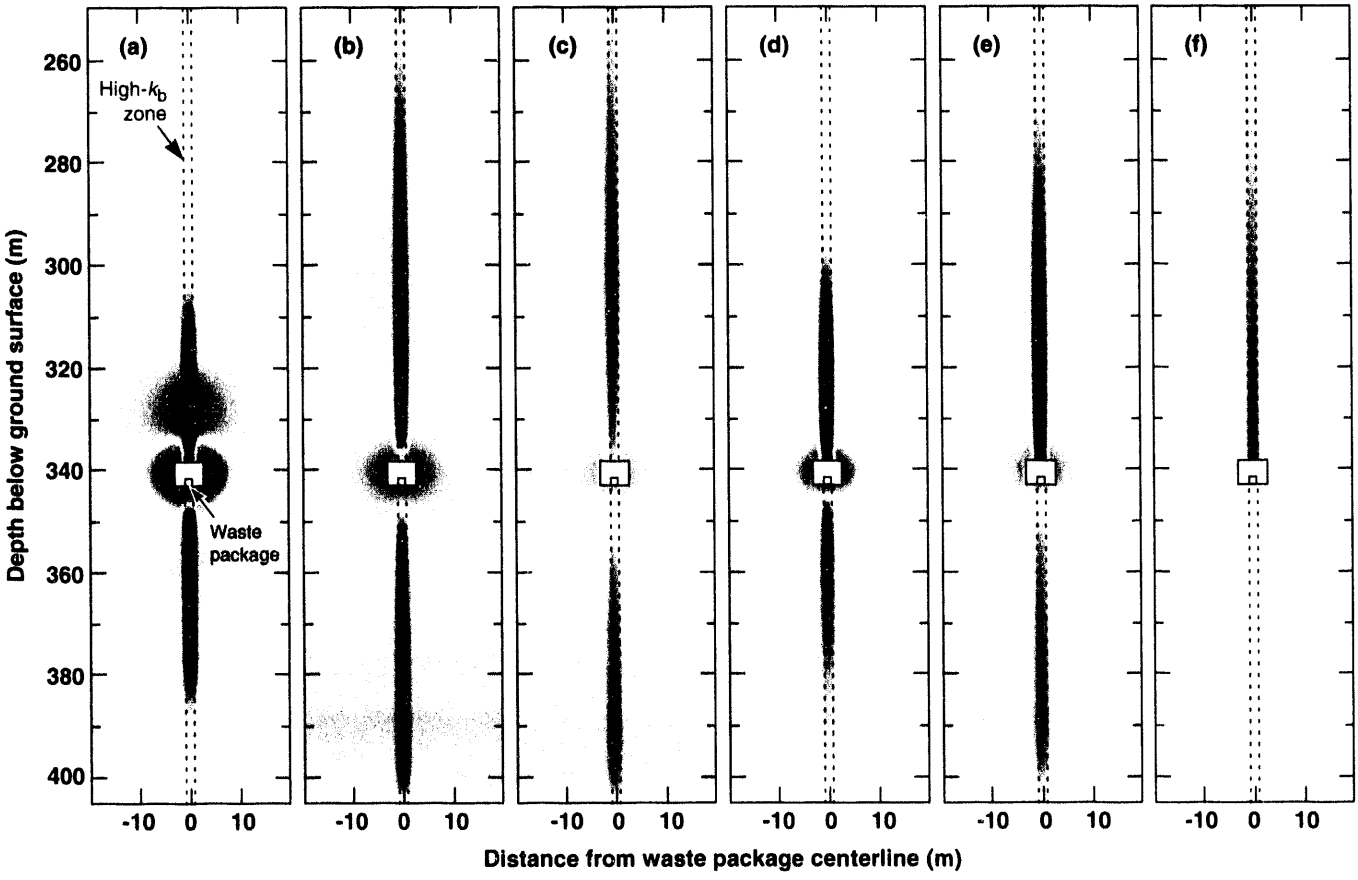

the top of the drift has dried out, focused vapor and condensate flow continues to cause refluxing in the high-k_h zone, resulting in a depression in the upper dry-out zone (Fig. 10b). Preferential heat conduction into the high-k_h zone continues to dry it out, and the manifestation of focused vapor and condensate flow on the dry-out zone gradually diminishes, until at 200 yr, it is no longer evident (Fig. 10c). Thereafter, the dry-out zone continues to develop as though the rock had a homogeneous k_h of 3.5 darcy, which is the bulk average of rock comprised of a 1.6-m-wide, 84-darcy zone and a 36.8-m-wide, 10-millidarcy zone.

For the second case of k_h heterogeneity, the duration of refluxing at the repository horizon (Figs. 10d and e) is considerably longer (40 yr) than in the first case (Fig. 10a). However, the ramifications of refluxing on WP performance are beneficial for the second case rather than deleterious as in the first case of k_h heterogeneity. Instead of potentially contributing to liquid contact on the WP, the refluxing zone in the pillar provides a conduit for condensate drainage through the repository horizon. This shedding of condensate around the emplacement drift may benefit WP performance by mitigating the buildup of condensate above the repository horizon. Notice that the refluxing zone continues to completely penetrate through the dry-out zone at 30 yr (Fig. 10d). As in the preceding example, the refluxing zone functions as a cooling fin that preferentially attracts heat flow from the neighboring rock. However, when the refluxing zone is removed from the heat sources (the WPs), as it is in the pillar, it takes longer for preferential heat flow to overwhelm the refluxing zone and begin to dry it out (Fig. 10e). At 200 yr, the manifestation of focused vapor and condensate flow on the dry-out zone is no longer evident, and the two cases have nearly identical dry-out zones (Figs. 10c and f). Thereafter, the dry-out zone continues to develop as though the rock had a homogeneous k_h of 3.5 darcy.

For 10-yr-old SNF and an AML of 49.2 MTU/acre, refluxing persists at the top of the drift for 65 yr (Fig. 11a), which is considerably longer than the 8.5-yr duration of refluxing for the 154.7-MTU/acre case (Fig. 10a). Notice that focused vapor and condensate flow continues to cause a depression in the upper dry-out front (Figs. 11b and c). It is important to note that this case is only able to generate marginal boiling conditions; consequently, there is insufficient heat to coalesce the dry-out zones between neighboring drifts. Moreover, the local heat flux from the WP is at best only sufficient to drive the re-wetting front in the high-k_h zone 1.5 m away from the top of the drift (Fig. 11b). After boiling ceases, condensate drainage in the high-k_h zone re-wets the top of the drift (Fig. 11c). However, the liquid saturation is less than the critical saturation for a mobile liquid phase in the fractures; consequently, the Equivalent Continuum Model (ECM) predicts matrix-dominated condensate drainage at 1000 yr (Fig. 11c). With the ECM, we cannot determine whether this condensate flux results in nonequilibrium fracture flow and dripping onto WPs.

We also analyzed a 49.2-MTU/acre case, with the subtle difference that it contains 20-yr-old SNF rather than the 10-yr-old SNF in the previous example. In past studies, we found that long-term, mountain-scale, thermo-hydrological performance primarily depends on AML and is less sensitive to SNF age. However, at the drift scale, sub-to-marginal boiling conditions result in thermo-hydrological behavior that is extremely sensitive to SNF age. For 20-yr-old SNF and an AML of 49.2 MTU/acre, refluxing (with a mobile liquid phase in the fractures) persists at the top of the drift for at least 1575 yr (Figs. 11d and e; note that 1575 yr is not shown). This thermal load generates marginal boiling conditions, which last only 160 yr, and is insufficient to coalesce the dry-out zones between neighboring drifts. There is also not enough heat to overwhelm the heat pipe and dry out the rock at the top of the drift. At 2534 yr, the liquid saturation in the high-k_h zone is quite high relative to ambient conditions (Fig. 11f), although it is less than the critical saturation for a mobile liquid phase in the fractures. However, with the ECM, we cannot determine whether this condensate flux results in nonequilibrium fracture flow and dripping onto WPs. The effect of gravity-driven refluxing is evident in Figs. 11e and f. Notice that, although focused condensate drainage ceases below the repository horizon, it continues above. The condensate buildup in the high-k_h zone persists for more than 5000 yr. To diagnose the potential for these effects to impact WP performance and radionuclide transport, *in situ* heater tests conducted under sub-boiling and above-boiling conditions will be required.[19,20]

Figure 12 shows the temperature history at various locations in the emplacement drift, including the WP surface, for AMLs of 49.2, 77.4, and 154.7 MTU/acre. This example is similar to the first case of k_h heterogeneity described above with one difference; for the high-k_h zone, k_h = 414 darcy rather than 84 darcy. We made this change to further enhance the degree of gas-phase focusing and the resulting duration of refluxing in the vicinity of the drift. For all three examples, focused vapor and condensate flow causes refluxing to persist in the high-k_h zone at the top of the drift. As long as refluxing persists at the top of the drift, it prevents the temperature there from exceeding the boiling point. For the 10-yr-old SNF, 49.2-MTU/acre case, refluxing persists at the top of the drift for more than 2000 yr, long after boiling has ceased (Fig. 12a). For the 30-yr-old SNF, 77.4-MTU/acre case, refluxing persists at the top of the drift for 150 yr (Fig. 12b), while for the 154.7-MTU/acre case, refluxing persists for 30 yr

(Fig. 12c). During the time that refluxing prevented the temperature in the high-k_b zone from exceeding the boiling point, temperatures throughout the rest of drift were well above boiling. For example, the temperature at the upper corner of the drift (only 2.8 m away from the high-k_b zone) managed to climb to 105, 111, and 144°C for the 49.2-, 77.4-, and 154.7-MTU/acre cases, respectively (Fig. 12). The corresponding WP surface temperatures were 121, 128, and 176°C (Fig. 12).

Figure 12. Temperature history at various locations in the emplacement drift for (a) 10-yr-old SNF, an APD of 57 kW/acre, and an AML of 49.2 MTU/acre; (b) 30-yr-old SNF, an APD of 57 kW/acre, and an AML of 77.4 MTU/acre; and (c) 30-yr-old SNF, an APD of 114 kW/acre, and an AML of 154.7 MTU/acre. Vertically oriented, 1.6-m-wide, 414-darcy zones are separated by 36.8-m-wide, 10-millidarcy zones.

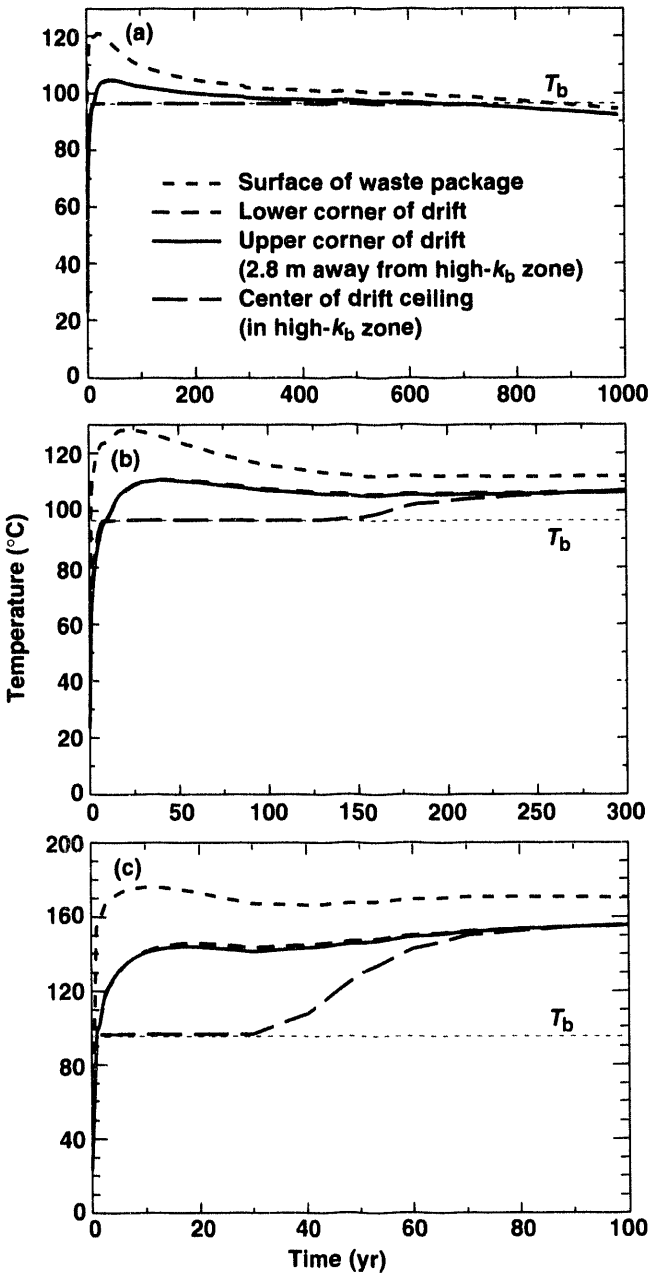

Based on experience with geothermal reservoirs, some have suggested that heat-pipe zones, spaced every 100 m, have the potential of convecting enough heat away from the repository to prevent its temperature from rising above the boiling point. However, we found in these examples, covering a wide range of AMLs, that the heat-pipe zone could not prevent the temperature at a location only 2.8 m away from exceeding the boiling point. Convection-dominated heat flow occurs in the heat-pipe zone, while in the neighboring rock, heat flow primarily occurs as heat conduction. Heat must be conducted from the heat sources (the WPs) to the heat-pipe zone in order for that zone to significantly influence repository temperatures. Heat cannot be conducted in relatively low thermal conductivity rock unless a significant temperature gradient is established, thereby causing temperatures away from the heat-pipe zone to be elevated above the boiling point.

III.F Hypothesis Testing

Much of the preceding discussion has emphasized repository-heat-driven processes that may increase the likelihood or quantity of liquid water contacting a waste package (WP) and driving radionuclide transport. However, depending on the thermal loading conditions, repository heat may also be instrumental in reducing the likelihood and quantity of liquid water reaching the repository for a considerable period of time. The Site Characterization Plan[15] includes the concept of a (300 to 1000 yr) period of "substantially complete containment" of radionuclides in WPs. This concept was developed largely on the basis of the assumption that, for the reference thermal loading conditions, a region of above-boiling temperatures surrounding WPs would keep them dry for 300 to 1000 yr. The "extended-dry" or "hot" repository is simply an extension of this concept.

Our model studies[5-7] show that the duration of boiling conditions is primarily dependent on the Areal Mass Loading of the repository and less sensitive to fuel age. For an Areal Mass Loading of 154.7 MTU/acre, we calculated the duration of the boiling period to be 11,500 yr at the center of the repository and about 4000 yr at the outer edge. We also found that boiling can result in a dry-out zone extending 300 m vertically (200 m above and 100 m below the repository horizon), with re-wetting of the repository horizon back to ambient conditions requiring more than 100,000 yr, long after boiling has ceased. Many of the calculations assumed averaged thermal loading conditions and did not represent how heterogeneity might cause focused vapor and condensate flow. However, more

recent calculations, which address the impact of heterogeneity and spatially varying thermal loading conditions, have yielded similar results for high thermal loads.[8]

It is important to point out that the calculations for the extended-dry repository (or for any other thermal load) have been conducted with idealized models that have not been validated and with limited data. The process of building confidence in our ability to *conservatively* predict performance is greatly facilitated by the use of the hypothesis tests we have listed below.[8] For the extended-dry repository, the critical questions involve how confidently we can predict the extent of above-boiling temperatures, whether such conditions correspond to the absence of mobile liquid water near WPs, and how long the dry-out zone persists after the end of the boiling period. These questions are addressed by the first four hypothesis tests. For a low-AML or "cold" repository, the critical question is to what extent can we neglect the hydrological impact of heat and thereby focus hydrological performance assessment on the ambient system. This question is addressed by the last three hypothesis tests, which are also crucial to any thermal loading concept. At this stage, we have identified the following hypothesis tests:

(1) whether heat conduction dominates heat flow,

(2) whether a region of above-boiling temperatures surrounding the repository corresponds to the absence of mobile liquid water at the WP environment,

(3) whether fracture density and connectivity are sufficient to promote rock dry-out due to boiling and condensate shedding,

(4) whether re-wetting of the dry-out zone back to ambient saturation lags significantly behind the end of the boiling period,

(5) whether mountain-scale, buoyant, gas-phase convection may eventually dominate moisture movement in the UZ,

(6) whether sub-repository-scale, buoyant, gas-phase convection dominates moisture movement at the repository, and

(7) whether heterogeneity results in focusing enough vapor flow and condensate drainage to cause persistent local liquid flow at the WP environment.

The first four hypotheses apply to a thermal loading strategy that utilizes heat to keep moisture away from WPs for some period of time. Ideally, the first four would be shown to be *true*. The first two apply to performance during the above-boiling period. If conduction dominates heat flow, we should be able to reliably predict the region of above-boiling conditions surrounding the repository, because the adequacy of heat flow models will depend primarily on accurate accounting of the thermal properties and thermal loading conditions, which are more readily determined and much less variable than many hydrological parameters. The second hypothesis being *true* is favorable because the absence of *mobile* water benefits WP integrity and eliminates advective liquid flow as a mechanism for mobilizing and transporting radionuclides.

The first four hypotheses also relate to post-boiling period performance, which benefits from a persistent zone of sub-ambient liquid saturation surrounding the repository. The first three hypotheses are the basis for predicting the spatial extent of the dry-out zone, and the fourth is the basis for how long that zone persists.

Hypotheses (5), (6), and (7) are critically important for any thermal loading strategy. It would be advantageous to repository performance if they were shown to be *false*. For a strategy that relies on a sub-boiling thermal load having a negligible impact on hydrological performance, this would be essential. The absence of significant buoyant, gas-phase convection and condensate focusing is beneficial to both above-boiling and below-boiling performance. These three hypotheses address the major repository-heat-driven sources of fracture flow, as well as a mechanism for building up the liquid saturation above the repository and re-wetting the dry-out zone. The only conclusive means of addressing these hypotheses is through long-term, *in situ* heater tests[19,20] and long-term monitoring of the thermo-hydrological behavior of the repository system.

IV. Conclusions

The radioactive heat-of-decay from spent nuclear fuel will play a dominant role in the performance of a potential repository at Yucca Mountain. Coupled hydrothermal-geochemical processes can strongly affect the composition and flow rates of gas and liquid around the waste packages. Waste package degradation, waste-form dissolution, and radionuclide release will critically depend on these processes. Repository heat will also play a dominant role in the evolution of the flow field that will drive gas-phase and liquid-phase transport. In addition, coupled hydrothermal-geochemical phenomena may significantly affect the performance of natural barriers underlying the repository. Depending on the thermal-loading management strategy (which will affect the design and operation of the repository) and site conditions, repository heat may either substantially increase the likelihood of water contacting waste packages and the magnitude of release and transport of radionuclides or preclude, or at least minimize, these effects for some period of time.

In our modeling studies, our approach has been to identify conditions that could potentially generate adverse performance. Accordingly, we have considered a wide range in bulk permeability and examples of heterogeneity that may be extreme. It is likely that the bulk permeability distribution at Yucca Mountain will be highly variable. Some of that variability will be random, while some may be correlated with discrete hydrological features such as

fault zones or hydrostratigraphic units. If the bulk permeability distribution includes significantly large regions in which the bulk permeability exceeds 10 darcy, then mountain-scale hydrothermal behavior will be more variable for low to intermediate AMLs than for high AMLs. If the bulk permeability distribution only includes values less than 1 darcy, then mountain-scale hydrothermal behavior will be less variable for all AMLs.

Because sub-repository-scale, buoyant, gas-phase flow only requires fracture networks to be connected over short distances, it has a greater likelihood of significantly impacting hydrological performance than does mountain-scale, buoyant, gas-phase flow. Depending on the waste package size and spacing, these effects can persist for thousands of years. For high AMLs, a large, persistent boiling zone suppresses the effects of sub-repository-scale, buoyant, gas-phase flow. For low AMLs, the extent of moisture movement is extremely dependent on the magnitude of sub-repository-scale, buoyant, gas-phase convection.

Zones of sharply contrasting bulk permeability may also influence condensate drainage. If the permeability contrast between neighboring zones is large enough, then gas-phase pressure differentials can drive water vapor into the high-permeability zone, where it condenses and drains, possibly causing persistent refluxing and water dripping onto waste packages. These effects can occur under both sub-boiling and boiling conditions. Because the high-permeability zones are competing for a finite quantity of vapor flow and condensate generation, there is a trade-off between the duration of refluxing and the number of locations where it can occur in the repository. If there are too many such zones, there will be insufficient condensate focusing to cause persistent refluxing at the repository horizon. The degree of focusing necessary to cause persistent refluxing limits the number of locations where it can occur. Therefore, it is unlikely that refluxing can dominate the overall thermal behavior in the repository.

An important observation is that the spatial variability of heating conditions and hydrological heterogeneity can cause local thermo-hydrological behavior to deviate substantially from averaged behavior. This was found to be particularly true for low to intermediate AMLs. Refluxing, resulting from focused vapor and condensate flow, was seen to be more persistent in the vicinity of waste packages for marginal boiling cases, sometimes continuing long after temperatures dropped below boiling. The persistence of refluxing near waste packages was found to decrease with increasing AML. For high AMLs, the effects of focused vapor and condensate flow virtually vanished, long before temperatures dropped below boiling. In this paper, we have begun to address condensate focusing that arises from preferential, gas-phase focusing. In future reports, we will address condensate focusing that arises from preferential, liquid-phase focusing of condensate, as well as from combinations of gas-phase and liquid-phase focusing, including consideration of infiltration from meteoric sources.

Some have equated the term "sub-boiling repository" with a repository system for which the hydrological impact of heat is insignificant. Some also define a "sub-boiling repository" to be one in which the average repository temperature is below the boiling point. Our analyses show that boiling conditions can persist around an emplacement drift even if the average repository temperature is well below the boiling point. Moreover, buoyant, gas-phase convection can drive significant vapor and condensate fluxes whether or not boiling ever occurs. The absence of local boiling conditions is an inadequate indicator of whether repository heat drives significant vapor and condensate flow. Average repository temperatures are an even poorer indicator of whether repository-heat-driven hydrothermal flow significantly impacts the performance of a low-AML repository. Diagnosing whether sub-boiling conditions can be equated with the absence of significant repository-heat-driven effects will require *in situ* heater tests conducted under sub-boiling as well as above-boiling conditions.

This work provides a context for understanding the relative importance of various hydrogeological properties and features that will be determined during site characterization. This work also shows that the challenge of adequately understanding repository-heat-driven, vapor and condensate flow is at least as formidable for sub-boiling conditions as for above-boiling conditions. Long-term *in situ* heater tests, conducted under both sub-boiling and above-boiling conditions, are required to determine the potential for the major repository-heat-driven sources of fracture flow to impact waste package performance and radionuclide transport.

Acknowledgments

The authors acknowledge the helpful and timely review of Ken Jackson. We also appreciate the assistance of Rick Wooten, who prepared the graphics and text layout, and the editorial assistance of Jay Cherniak. We also thank Marion Capobianco for assisting in the text layout. This work was supported by the Near-field Hydrology Task (WBS 1.2.2.2.2) of the Yucca Mountain Site Characterization Project. Work performed under the auspices of the U.S. Department of Energy by Lawrence Livermore National Laboratory under Contract W-7405-Eng-48.

References

1. Montazer, P., and W.E. Wilson, "Conceptual Hydrologic Model of Flow in the Unsaturated Zone, Yucca Mountain, Nevada," Water Resources Investigation Report 84-4345, U.S. Geological Survey (1984).

2. Klavetter, E.A., and R.R. Peters, "Estimation of Hydrologic Properties of an Unsaturated Fracture Rock Mass," *SAND84-2642*, Sandia National Laboratories, Albuquerque, NM (1986).

3. Buscheck, T.A., J.J. Nitao, and D.A. Chesnut, "The Impact of Episodic Nonequilibrium Fracture-Matrix Flow on Geological Repository Performance," *Proceedings American Nuclear Society Topical Meeting on Nuclear Waste Packaging (Focus 91)*, Las Vegas, NV, Sept. 30–Oct. 2, 1991. Also, *UCRL-JC-106759*, Lawrence Livermore National Laboratory, Livermore, CA (1991).

4. Nitao, J.J., T.A. Buscheck, and D.A. Chesnut, "Implications of Episodic Nonequilibrium Fracture-Matrix Flow on Repository Performance," *Nuclear Technology*, Vol. 104, No. 3, pp. 385–402 (1993).

5. Buscheck, T.A., and J.J. Nitao, "The Impact of Thermal Loading on Repository Performance at Yucca Mountain," American Nuclear Society, *Proceedings Third International High-Level Radioactive Waste Management Conference*, Las Vegas, NV, April 12–16, 1992. Also, *UCRL-JC-109232*, Lawrence Livermore National Laboratory, Livermore, CA (1992).

6. Buscheck, T.A., and J.J. Nitao, "The Impact of Repository-Heat-Driven Hydrothermal Flow on Hydrological Performance at Yucca Mountain," American Nuclear Society, *Proceedings Fourth International High-Level Radioactive Waste Management Conference*, Las Vegas, NV, April 1993. Also, *UCRL-JC-112444*, Lawrence Livermore National Laboratory, Livermore, CA (1993).

7. Buscheck, T.A., and J.J. Nitao, "Repository-Heat-Driven Hydrothermal Flow at Yucca Mountain, Part I: Modeling and Analysis," *Nuclear Technology*, Vol. 104, No. 3, pp. 418–448 (1993).

8. Buscheck, T.A., and J.J. Nitao, "The Impact of Repository Heat on Thermo-Hydrological Performance at Yucca Mountain," *Proceedings American Nuclear Society Topical Meeting on Site Characterization and Model Validation (Focus 93)*, Las Vegas, NV, Sept. 26–30, 1993. Also, *UCRL-JC-114791*, Lawrence Livermore National Laboratory, Livermore, CA (1993).

9. Pruess, K., Y.W. Tsang, and J.S.Y. Wang, "Numerical Studies of Fluid and Heat Flow near High-Level Nuclear Waste Packages Emplaced in Partially Saturated Fractured Tuff," *LBL-18552*, Lawrence Berkeley Laboratory, Berkeley, CA (1984).

10. Pruess, K., J.S.Y. Wang, and Y.W. Tsang, "On Thermohydrologic Conditions near High-Level Nuclear Wastes Emplaced in Partially Saturated Fractured Tuff, Part 1: Simulation Studies with Explicit Consideration of Fracture Effects," *Water Resources Research*, Vol. 26, No. 6, pp. 1235–1248 (1990).

11. Nitao, J.J., "V-TOUGH - An Enhanced Version of the TOUGH Code for the Thermal and Hydrologic Simulation of Large-Scale Problems in Nuclear Waste Isolation," *UCID-21954*, Lawrence Livermore National Laboratory, Livermore, CA (1989).

12. Pruess, K., "TOUGH User's Guide," *NUREG/CR-4645*, Nuclear Regulatory Commission (1987).

13. Peters, R.R., E.A. Klavetter, I.J. Hall, S.C. Blair, P.R. Hellers, and G.W. Gee, "Fracture and Matrix Hydrologic Characteristics of Tuffaceous Materials from Yucca Mountain, Nye County, Nevada," *SAND84-1471*, Sandia National Laboratories, Albuquerque, NM (1984).

14. DOE (U.S. Dept. of Energy), "Yucca Mountain Project Reference Information Base," *YMP/CC-0002 (Version 04.002)*, Nevada Operations Office, Las Vegas, NV (1990).

15. SNL (Sandia National Laboratories), "Site Characterization Plan - Conceptual Design Report," *SAND84-2641*, Sandia National Laboratories, Albuquerque, NM (1987).

16. Pruess, K., and Y.W. Tsang, "Modeling of Strongly Heat-Driven Processes at a Potential High-Level Nuclear Waste Repository at Yucca Mountain, Nevada," *Proceedings Fourth International High-Level Radioactive Waste Management Conference*, Las Vegas, NV (April 1993).

17. Nitao, J.J., and T.A. Buscheck, "Analysis of the Potential for Large-Scale, Repository-Driven Convection at Yucca Mountain," in preparation, Lawrence Livermore National Laboratory, Livermore, CA (1994).

18. Buscheck, T.A., S.F. Saterlie, and J.J. Nitao, "Evaluation of Thermo-Hydrological Performance in Support of the Thermal Loading Systems Study," American Nuclear Society, *Proceedings Fifth International High-Level Radioactive Waste Management Conference*, Las Vegas, NV (May 1994). Also, *UCRL-JC-115352*, Lawrence Livermore National Laboratory, Livermore, CA (1994).

19. Buscheck, T.A., D.G. Wilder, and J.J. Nitao, "Large-Scale *In Situ* Heater Tests for the Characterization of Hydrothermal Flow at Yucca Mountain," American Nuclear Society, *Proceedings Fourth International High-Level Radioactive Waste Management Conference*, Las Vegas, NV, April 1993. Also, *UCRL-JC-112445*, Lawrence Livermore National Laboratory, Livermore, CA (1993).

20. Buscheck, T.A., D.G. Wilder, and J.J. Nitao, "Repository-Heat-Driven Hydrothermal Flow at Yucca Mountain, Part II: Large-Scale *In Situ* Heater Tests," *Nuclear Technology*, Vol. 104, No. 3, pp. 449–471 (1993).

21. Weeks, E.P., "Gas-Phase Flow at Yucca Mountain," presentation to the National Academy of Sciences' Committee on the Technical Basis for Yucca Mountain Standards, National Research Council, December 16, 1993.

22. Weeks, E.P., personal communication, U.S.G.S., Denver, CO (1993).

23. Philip, J.R., and D. A. de Vries, "Moisture Movement in Porous Materials under Temperature Gradients," *Transactions, American Geophysical Union*, Vol. 38, No. 2, pp. 222–232 (April 1957).

24. Cass, A., G.S. Campbell, and T.L. Jones, "Enhancement of Thermal Water Vapor Diffusion in Soil," *Soil Science Society of America Journal*, Vol. 48, pp. 25–32 (1984).

25. Nitao, J.J, R.M. Bradford, and W.J. O'Connell, "Modeling the Heterogeneity of Condensate Flux through a Heated Repository," *UCRL-ID-115412*, Lawrence Livermore National Laboratory, Livermore, CA (1993).

DATE
FILMED
10/21/94
END